3D modelling of underwater archaeological artefacts

Natalia Gawlik

NORWEGIAN UNIVERSITY OF SCIENCE AND TECHNOLOGY
DEPARTMENT OF CIVIL AND TRANSPORT ENGINEERING

Report Title: 3D modeling of underwater archaeological artifacts	Date: 30.06.2013		
	Number of pages (incl. appendices): 98		
	Master Thesis	x	Project Work
Name: Gawlik Natalia			
Professor in charge/supervisor: Knut Ragnar Holm			
Other external professional contacts/supervisors: Martin Ludvigsen, Øyvind Ødegård			

Abstract:

Underwater photogrammetry is a good alternative to traditional archaeological excavations, which are often less accurate and very destructive to underwater artefacts Furthermore the photogrammetric principles applied with the Remotely Operated Vehicles allows us to explore objects that are at very great depths. For this thesis proposes a stereo camera system unit was designed in order to extract three-dimensional data from digital images. This stereo system unit consists of two cameras, two camera housings and a stereo bar mounted on a pan/tilt unit. Relative positions between these two cameras will provide us the external orientation data and in consequence it might solve the problem caused by the lack of ground control data on the underwater site.

This master thesis also gives an insight into some of the mathematical background of photogrammetry, especially an influence on the intrinsic camera parameters caused by the air-glass-water interface is described. The underwater images are dark, murky and of poor quality due to a difficult conditions under water. In order to improve the perception of the underwater images a script based on histogram stretching of a few colour models are proposed.

The primary subject of this thesis was a 3D modelling of the underwater shipwreck believed to be *Den Waagende Thrane (The Waking Crane)*, which sunk in the Trondheim harbour in 1713. However due to technical problems this particular measurement has not been performed. Two other underwater objects were surveyed from the offshore based on the previously prepared data acquisition plans. In result a few three-dimensional models were created using different settings and a detailed analysis of the quality and utility of these models were conducted.

Keywords:

1. Underwater photogrammetry
2. 3D modeling
3. Underwater archeology
4. Marine Technology

Ngawlik

MASTER THESIS

Spring 2014
for

Natalia Gawlik

3D modelling of underwater archaeological artefacts

Project description:

The aim of this thesis is to find the most optimal way to measure and create an accurate 3D digital model of underwater archaeological artefacts using digital photogrammetry. Measurement of the ancient shipwreck will be conducted by remotely operated vehicle. The thesis will include a description of the problem, the current procedures, planning, underwater survey and 3D model generation.

Key words:

Underwater photogrammetry, 3D modelling, underwater archaeology, marine technology

Supervisors:

Knut Ragnar Holm, Martin Ludvigsen, Øyvind Ødegård

Abstract

Underwater photogrammetry is a good alternative to traditional archaeological excavations, which are often less accurate and very destructive to underwater artefacts Furthermore the photogrammetric principles applied with the Remotely Operated Vehicles allows us to explore objects that are at very great depths. For this thesis proposes a stereo camera system unit was designed in order to extract three-dimensional data from digital images. This stereo system unit consists of two cameras, two camera housings and a stereo bar mounted on a pan/tilt unit. Relative positions between these two cameras will provide us the external orientation data and in consequence it might solve the problem caused by the lack of ground control data on the underwater site.

This master thesis also gives an insight into some of the mathematical background of photogrammetry, especially an influence on the intrinsic camera parameters caused by the air-glass-water interface is described. The underwater images are dark, murky and of poor quality due to a difficult conditions under water. In order to improve the perception of the underwater images a script based on histogram stretching of a few colour models are proposed.

The primary subject of this thesis was a 3D modelling of the underwater shipwreck believed to be *Den Waagende Thrane (The Waking Crane)*, which sunk in the Trondheim harbour in 1713. However due to technical problems this particular measurement has not been performed. Two other underwater objects were surveyed from the offshore based on the previously prepared data acquisition plans. In result a few three-dimensional models were created using different settings and a detailed analysis of the quality and utility of these models were conducted.

Acknowledgments

This master thesis involved many people for whom I would like to express my sincere gratitude.

I would like to express my sincere gratitude to my main supervisor Knut Ragnar Holm for providing me the possibility and ability to do this thesis. I would like to thank him for all the time, encouragement, valuable guidance and support.

I am grateful to my immediate supervisor Martin Ludvigsen for the assistance and help to do this project and for all professional consultations.

I would also like to acknowledge with great appreciation the help and expertise always available from Mauro Candeloro and Frode Volden.

I am grateful to Øyvind Ødegård for support and help regarding the project.

I am grateful to my colleague Torbjørn Auglænd Vilhelmsen for his assistance with the measurements.

Glossary

3D model – a mathematical representation of a three dimensional object.

AUV - Autonomous Underwater Vehicle – a robot submarine that does not require any input data from an operator to travel underwater

Aperture (F-number) – a unit that defines the amount of light passing through the camera.

Depth of Field - the zone where the object is acceptably sharp in an image.

DLT - Direct Linear Transformation – an algorithm commonly used in the camera calibration in order to calculate the three dimensional position of a point by measuring the same point on two images.

DTM – Digital Terrain Model – a continuous digital representation of the ground surface or the terrain

Focal length – a distance between the centre of a lens and the focal point.

HiSAS 1030 - Synthetic Aperture Sonar (SAS) - a measuring system that provides ultra-high-resolution images and bathymetry data of the seabed. Image data is created by a combination of number of acoustic pings received by the sonar.

Histogram – a graphical representation of the pixel intensity values in of a digital image.

HSI colour space – a colour space which represents every colour with the Hue, Saturation and Intensity components in an RGB colour model.

HSV colour space – a colour space which represents every colour with the Hue, Saturation and Value components in an RGB colour model.

ROV – Remotely Operated Underwater Vehicle – remote-controlled robot submarine which is connected to a ship by a cable or a tether. The vehicle allows us to explore the sea without leaving the deck of a ship.

LSM - Least Squares Method – a procedure used to determine the best fit of the statistical data to mathematical function.

Mosaic (photomosaic, ortophotomosaic) - a composition image created from individual geometrically corrected digital photographs.

Perspective camera model (pinhole camera model) – a model in which the relationship between the object and its projection on the image is described by the perspective projection.

Polarization filter – a filter that can be mounted on a camera lens in order to reduce the glare in glass or water or decrease the haze.

RGB colour model – an additive colour model composed of the Red, Green and Blue channel.

y − parallax – „the difference of a point in a y direction is the algebraic difference of the distances of the two images from their respective photo nadirs measured in a horizontal plane and parallel to the stereo base" (Thompson, 1966).

List of figures

List of tables

List of attachments

Appendix 1 The model of the shovel created based on the interpolation technique with generic texture using average value of the all pixels (available electronically in 3D PDF with this thesis)

Appendix 2 The model of the shovel created in Geomagic (available electronically in 3D PDF with this thesis)

Appendix 3 The model of the pipeline created based on the interpolation technique with generic texture using average value of the all pixels (available electronically in 3D PDF with this thesis)

Table of Contents

1. Introduction

Traditional, manual deep water archaeological excavations are expensive, complex and may damage the investigated object. Current efforts aim to preserve underwater heritage, thus photogrammetry turns out to be the most suitable choice. The principle of underwater photogrammetry does not differ from traditional photogrammetry, but it is essential to take into account certain elements that may cause disturbance, such as light refraction effects due to two media boundary and the presence of the camera housing. The important advantage of using photogrammetry in underwater surveys in comparison with the use of other techniques is its simplicity of implementation and the diversity of potential results (Drap, P., 2012). Considering the depth photogrammetric measurements can be conducted by scuba divers or Remotely Operated Vehicles (ROVs). However use of modern techniques such as ROVs, computer technology and sophisticated tools, enhance productivity and safety in marine archaeological surveys and excavations. (Jasinski, et al., 1995). Moreover this method requires little time and does not require specific personnel, thus greatly reducing the expenses in a context where time and costs of intervention are extremely high (Drap, P., 2012).

1.1 Task description

The aim of this thesis is to find the most optimal way to measure and create an accurate 3D digital model of underwater archaeological artefacts using digital photogrammetry. Measurement of the ancient shipwreck will be conducted by remotely operated vehicle. The thesis will include a description of the problem, the current procedures, planning, underwater survey and 3D model generation.

1.2 Description of the object

The historical shipwreck is located in the Trondheim harbour approximately 60 meters deep (figure 1). The shipwreck was found in the area around Munkholmen in 1995 by a scuba diver. The extraordinary preservation of the underwater shipwreck is probably caused by a high freshwater content in the Trondheim harbour due to the Nidelva river discharge and a small activity of the marine wood-borers. The shipwreck is approximately 18 m long and it is protruding up to 20 cm off the seabed. The bow and the other wooden structures are still visible on the seabed. According to F. Søreide (2000) "the elements of a hatch can be seen near the centre and parts of the stem are still standing up at the front. By the stern there are traces of ceramics, yellow bricks and lead".
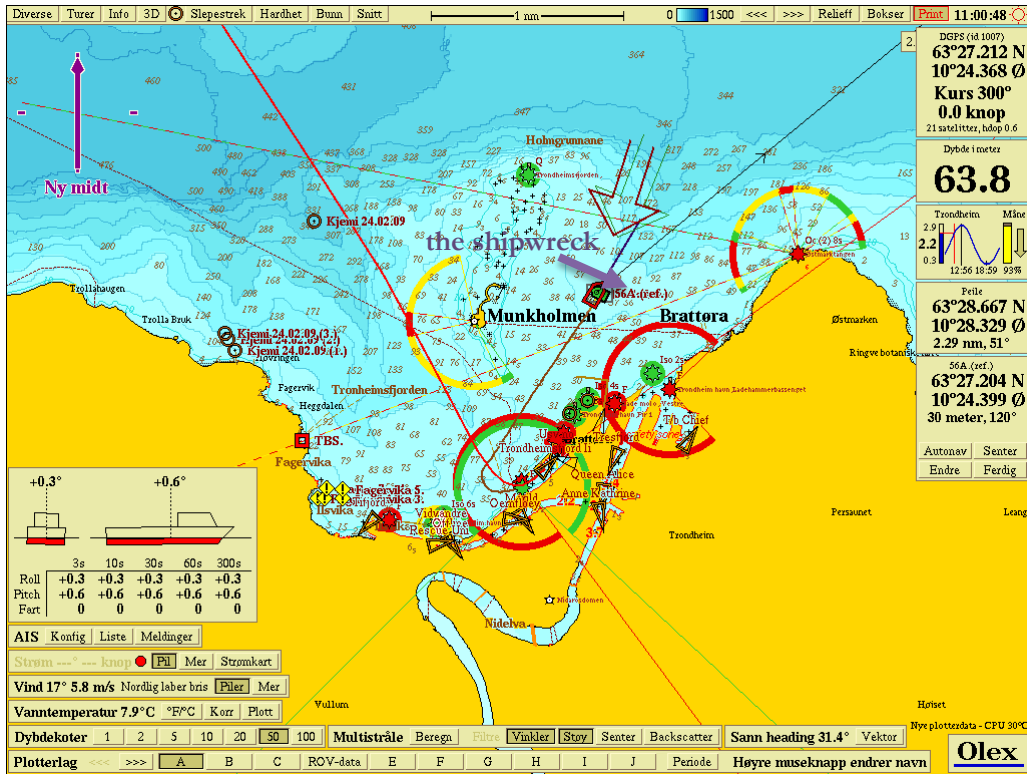
Figure 1 *Position of the shipwreck in the Trondheim harbour.*

The shipwreck was investigated by the Hyball ROV equipped with Simrad 971 scanning sonar and a video camera. The samples collected on the site was examined and dated back to the 17th or 18th century. According to the Official Norwegian archives, the shipwreck could be *Den Waagende Thrane (The Waking Crane)*, which sank in 1713 in Trondheim harbour. The site plan, shown in the figure 2 was made based on acoustic measurements and video images (Søreide, 2000), (Søreide, 2011), (Ødegård, et al., 2013).

UNIDENTIFIED SHIPWRECK
MUNKHOLMEN TRONDHEIM
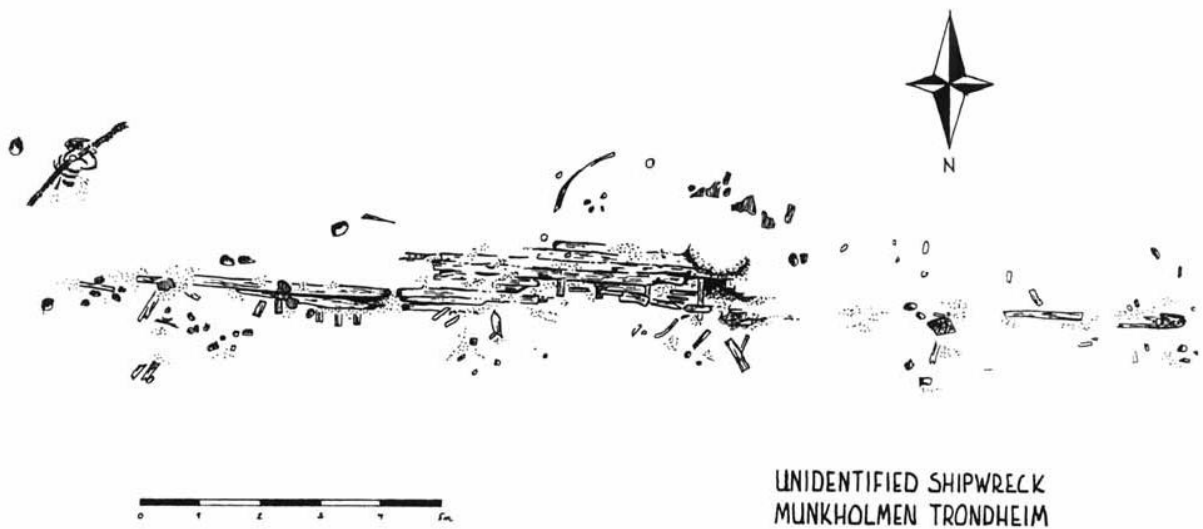
Figure 2 *General site plan of the shipwreck - site (drawing: S. Carpenter) (Søreide, 2000)*

1.3 Problems and limitations

Underwater photogrammetry has some key differences compared to conventional photogrammetry methods. These are as follows:

- Limited access to the underwater object,
- No operational control on data acquisition when measurements are conducted by a unqualified scuba diver,
- Poor illumination and colour absorption,
- Three-interface (water, glass and air) data collection affects intrinsic parameters of the camera and automatic photogrammetric process,
- Significant light diffusion (the visibility in the water decreases with an increasing distance from the object)
- No control point establishment (Skarlatos & Rova, 2010), (Skarlatos, et al., 2010), (Diamanti, et al., 2012).

Camera calibration is a major problem connected with underwater photogrammetry. Refraction caused by air-glass-water interface result in a high distorted images and it must be taken into consideration during camera calibration process. However according to the Young-Hoo Kwon (1998) the refraction error caused by two different media can be covered by radial distortion. Consequently standard photogrammetric calibration software to calibrate the digital cameras and their housing can be used (Kwon, 1998).

Establishment of the control under the water is mostly impossible and very inaccurate. Trilateration methods conducted by a traditional tape measurements can hardly never exceed required accuracy. Control points established underwater should be measured with a 1/3 accuracy over the whole block. At present mostly scale bars and vertical buoys are used in underwater survey to set up a scale and a vertical axis of the object. External orientation (coordinates of the projection centre X, Y, Z and the three rotation angles) of every camera can be measured by GPS and IMU systems. Jon Henderson (2013) created a stereo system which employ these two positioning devices to acquire precise position of every underwater photograph. However this method increases significantly cost of the measurement (Skarlatos, et al., 2010), (Eric, et al., 2013).

Surveyors have no control on data acquisition when underwater measurements are conducted by scuba divers. Additionally the operative time during this kind of surveys is very limited (less than 30 min at depth over 30 meters). It is not possible to perform all the underwater procedures correctly in very limited time frame. Moreover, according to the Norwegian work-safety regulations, in Norway scuba divers can only dive to 30 m (Jasinski, et al., 1995), (Eric, et al., 2013).

The last issue that can cause problems in underwater survey are occlusions and moving objects (the fish, the seaweed, the particles suspended in the water) which can result in an inaccurate or incomplete product. Covered objects will not be seen on the photographs and moving objects can result in failure in the automatic photogrammetric process. Sometimes the underwater object cannot be fully recovered unless the overlaid layer is excavated (Søreide, 2000), (Skarlatos, et al., 2010).

1.4 Previous work and existing data

The historical shipwreck was first found and measured during the test run of Side Scan Sonar in 1981. More complex examinations were conducted after 1995 by Fredrik Søreide. The shipwreck was measured and recorded. Additionally a piece of wood was collected to examine its age and dated back to 17th or 18th century. In the following years the shipwreck have been the subject of multiple researches. In 1996 a sidesonar survey was carried out by researchers from the NTNU in Trondheim to measure both the historical shipwreck and the surrounding site. As a result of this investigation a few new wrecks were found. The historical shipwreck which is described as no 1 in figure 3 was believed to be Den Waagende Thrane and it was examined in detail. The lengths of the object and surrounded artefacts were positioned and measured by acoustic method and additionally with measuring rod. The historical shipwreck was partly excavated. A few parts of the stern area were excavated and carried out to the surface by the ROV. Sediment covering the shipwreck was removed in order to expose lower parts of the shipwreck. A layer of boards were removed and the lower layer of boards and deck girders were examined in detail. Additionally a few new objects were found on the site: glass, pieces of ceramic, lead, iron and wood. Some of the objects were carried to the surface for further examination. Unfortunately due to lack of sufficient evidence the shipwreck could not be unambiguously identified as *Den Waagende Thrane*. Afterwards the shipwreck was measured by combination of two techniques: underwater positioning system and photogrammetry. This method provided fast and good results in comparison with previous attempts (Søreide, 2000), (Søreide, 2011).
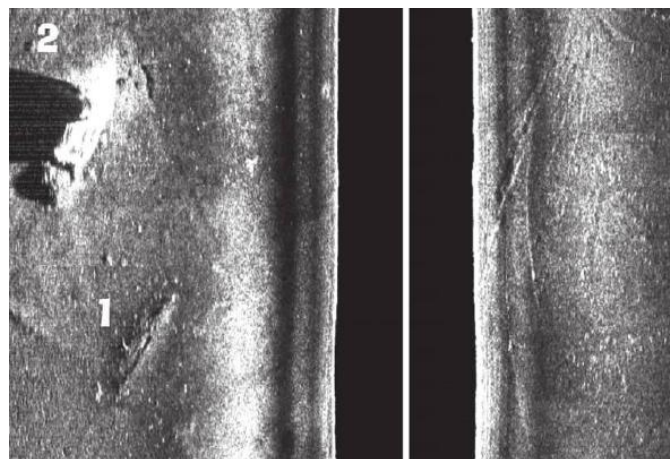
Figure 3 *Sonar image with the historical wreck (1) and other, modern wreck (2) (Søreide, 2000)*

Applied Underwater Robotics Laboratory from NTNU and Norwegian Defence Research Establishment conducted surveys in Trondheim harbour in December 2012. During this cruise the historic shipwrecks in Trondheim harbour were measured using the Autonomous Underwater Vehicle (AUV) equipped with the Synthetic Aperture Sonar (SAS) system. One of the research area was focused on the historical shipwreck site which is subject of this thesis. Survey was performed between Munkholmen and Lade peninsula. Investigations resulted in a high resolution HiSAS 1030 imagery mosaic of the investigated area (figure 4). The HiSAS imagery allows to recognize objects smaller than 10 cm.

Figure 4 *Map of Trondheim harbour with HiSAS 1030 imagery mosaic (Ødegård, et al., 2013)*

The historical site were measured at different angles and ranges and a few data sets were acquired (figure 5). The distinctive line in the middle of images is a partially exposed keelson. The shadows occurred on a few images point out that the shipwreck is a mound rising from the seabed. According to Øyvind Ødegård (2013) "on the images 5-8 it is possible to see some vague features running parallel with the keelson with some shorter features perpendicular on top of them. This was later identified as probable planking and frames attached to the keelson". The historical shipwreck profile created using the barometric data shown in the figure 6 implies that more remains of the historical shipwreck may be buried in the sediments (Ødegård, et al., 2013).
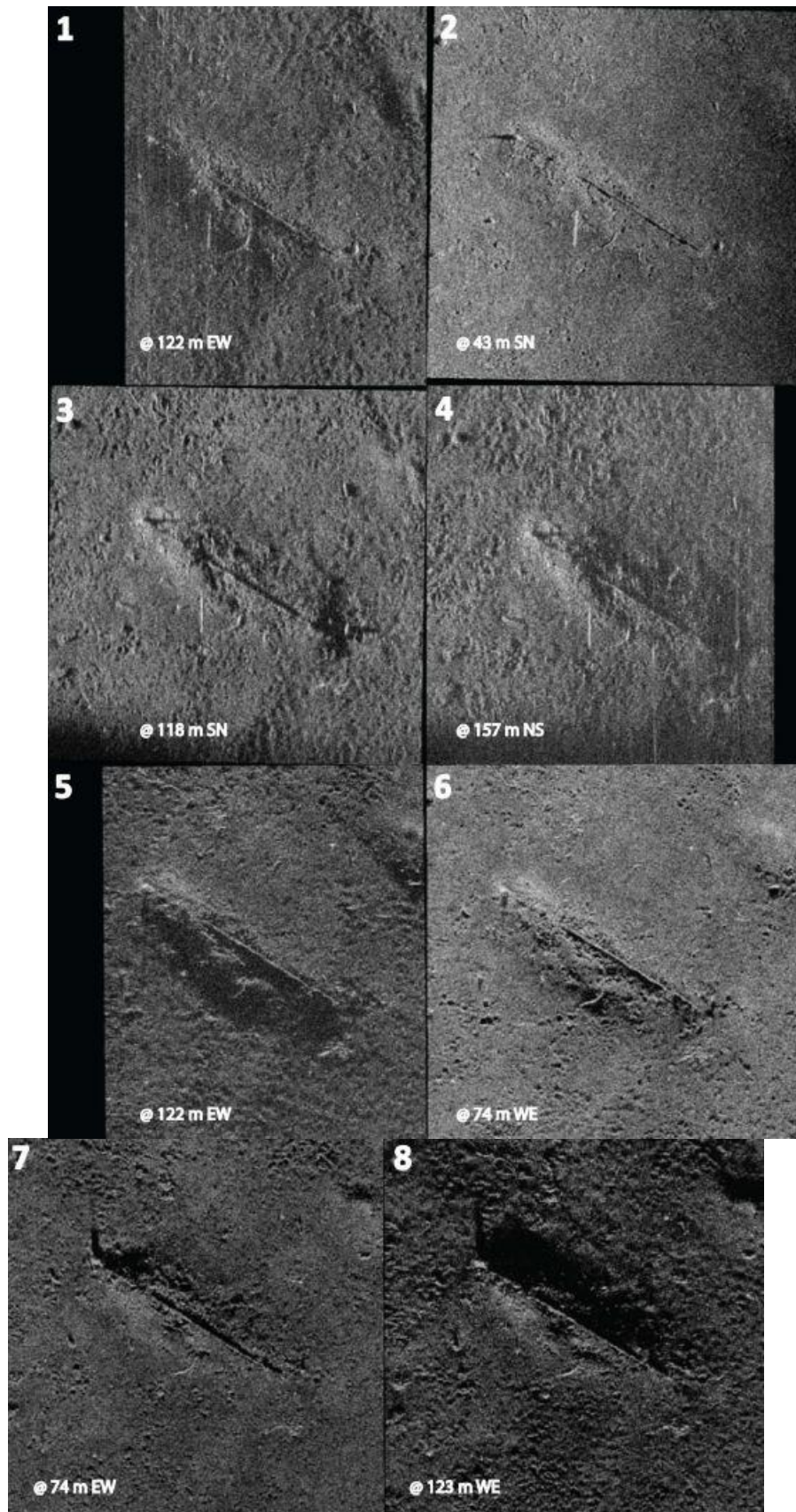
Figure 5 _HiSAS imagery of the historic shipwreck site (Ødegård, et al., 2013)_
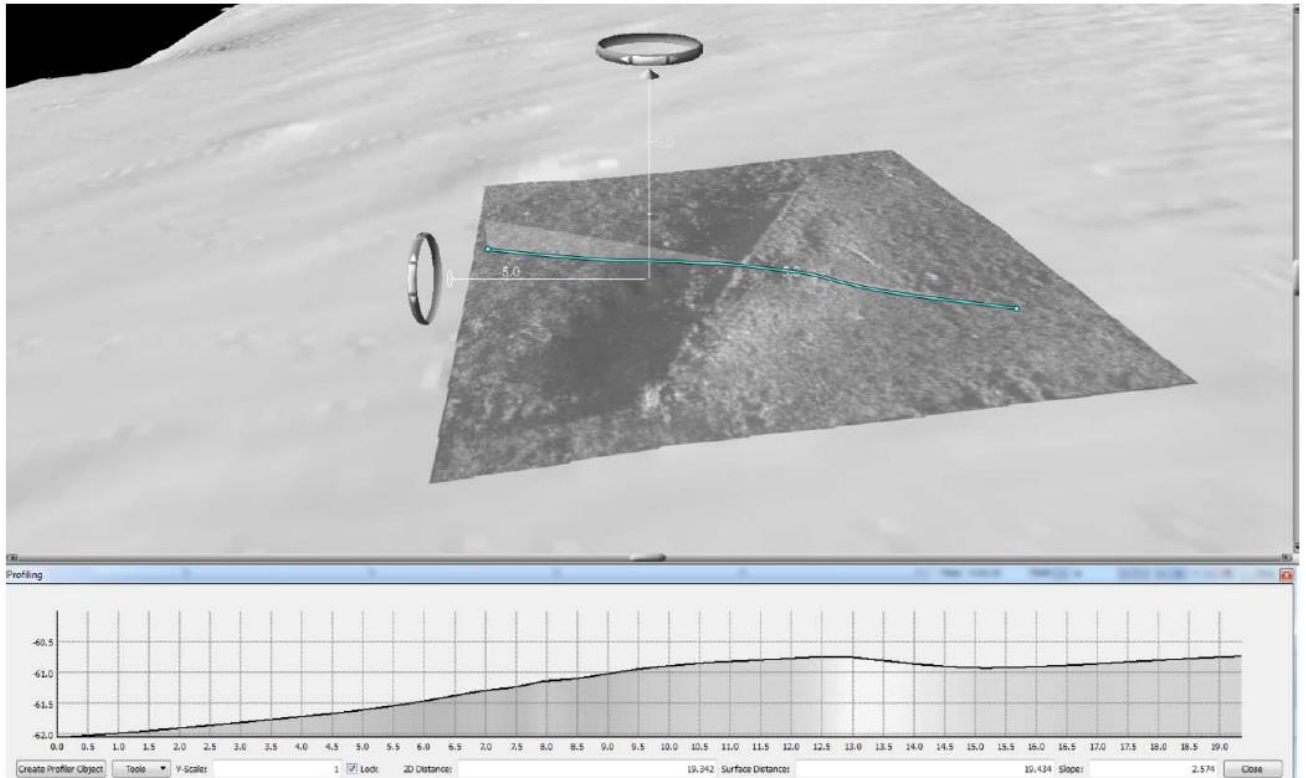
Figure 6 *HiSAS image of the historical shipwreck draped on bathymetric model (Ødegård, et al., 2013)*

Nowadays the historic shipwreck is the subject of various examinations carried out by NTNU researchers and students.

2. Theory

This chapter describes necessary theory concerning the underwater survey. In the first part important laws and regulations regarding underwater surveying in Norway is described. Furthermore first attempts to introduce photogrammetric methods in underwater survey and a few further underwater photogrammetry projects used for different applications are presented. Next the camera calibration procedure and the description of the intrinsic parameters of the camera is given. Additionally the impact of refraction caused by the water-glass and the glass-air interface on the intrinsic parameters under water is presented. In addition, parameters of the stereo camera system are shown and the parameters stability under water is discussed. The influence of light attenuation, scattering, non-uniform illumination and colour absorption and low image contrast on the underwater imagery is given. Finally the underwater image processing techniques are described.

2.1 Laws and regulations

There are two main legal acts regulating the cultural heritage in Norway: The Convention on the Protection of Underwater Cultural Heritage (UNESCO) and Act of 9 June 1978 No.50 Concerning the Cultural Heritage.

The regulations in The Convention on the Protection of Underwater Cultural Heritage (2011) apply to protect and preserve the underwater cultural heritage without any unnecessary change of their original place. All activities connected with the underwater cultural heritage should be authorized according to the protection of the heritage. Additionally significant actions should be undertaken in order to preserve and improve of the quality of underwater cultural heritage. Any activities related to the underwater cultural heritage should not affect the object more than necessary. Moreover chosen survey methods should not be destructive for the underwater heritage. The underwater object should not be recovered without a specific reason. If the excavation of the underwater object is required to be done, the methods and techniques used during the process can not affect or destroy the underwater object (UNESCO, 2011).

Act of 9 June 1978 No.50 Concerning the Cultural Heritage introduced by the Ministry of Climate and Environment forbid to "take any action that may damage, destroy, move, change, cover conceal or in any other way unduly disfigure any monument or site. Monuments and sites are automatically protected by law" (MCE Ch. II §3, 1978).

Regulations concerned about shipwrecks and underwater monuments and sites are described in chapter IV. Ship Finds and Protection of Vessels. The chapter apply that both cultural heritage on land and under the water must be protected in the same manner. Any ships, hulls, gear, cargo and anything what has been found n on board, or parts of such

objects that are more than 100 years old belongs to the state. Moreover the state is allowed to excavate, move, examine objects and perform other activities in order to preserve the object that irrespective of the owner. Any measurements of the underwater cultural heritage cannot be carried out without necessary permission from the competent authority by the owner or others. In a case when the permission is granted by the state any measurements cannot damage the underwater cultural heritage. In addition measurements must be performed in accordance with the appropriate regulations (MCE Ch. IV §10, 1978).

Summary:

Marine archaeological investigations must be carried out before construction work by proper authorities. Any damage or change of archaeological sites and monuments should be avoided. The owner of the construction is responsible for the costs of such investigations. If the cost is found to be extraordinary high, the Norwegian State may reimburse or pay for the whole or parts of the investigation. The cultural remains on land and under the sea should be protected in the same way.

2.2 Related work

The first attempts to apply photogrammetric procedures in underwater archaeology started in the 60s. Early surveys were performed using various submarines and semi-metric or metric film-based cameras. With the technology development, underwater measurements have become more accessible, faster and less time-consuming. Presently underwater photogrammetry is used in the diverse areas such as underwater archaeology, underwater surveys, fishery, biology and t ne he petroleum industry (Drap, P., 2012), (Drap , et al., 2005).

Underwater stereo-video camera systems can be widely used in fisheries researches and in monitoring marine fauna populations. Underwater photogrammetry allows us to count and measure length of fish without the need to capture and handle them. The present surveys strive to automate the measuring process and reduce the time of post-processing (Havrey, et al., 2003), (Shortis & Harvey, 1998).

Underwater stereo photogrammetry is often used to study of the population dynamics of red coral. In comparison to traditional, manual methods, photogrammetric techniques are less likely to destroy the fragile coral. The photogrammetric system allows us to acquire in an efficient and precise way data for the analysis. This method provides us reliable data about colony sizes, occurrence of breakage of colonies and the occurrence of necrosis (Drap, et al., 2013).

Photogrammetry is successfully used in underwater archaeology. This method provides higher accuracy data and is less time-consuming than traditional archaeological underwater measurements. At present the remotely or autonomous operated vehicles allows us to survey in very deep waters which were not possible previously. The photographs taken by the vehicles may be used to generate an ortophotomosaic or a 3D model of the underwater artefacts. The submerged Pavlopetri town in Greece was surveyed using the stereo-vision system. The system uses a stereo-vision diver platform which consists of the two cameras, two LED strobe lights, the depth sensor and the GPS receiver. The position of each photograph is measured and combined with mapping techniques to create high-resolution 2D photomosaics and 3D models. The principle of this technique can be also used in ROV surveys at great depths. However the accuracy of the marine navigation systems are not that as high as GPS measurements (Eric, et al., 2013), (Henderson, et al., 2013), (APOMAB, 1999).

Aerial photogrammetry principles may be applied in underwater photogrammetric measurements. The main differences between underwater and aerial surveys are the distance to the seabed and the immersion in water. This approach were successfully used both in the VENUS European Project (Virtual ExploratioN of Underwater Sites) and the survey of the antique ship from Phanagoria. In VENUS project the Digital Terrain Model (DTM) was created from nadir photographs taken by the ROV. In the other project, the antique ship was covered by both vertical and oblique images. The camera was fixed on a small platform which provides a stable position of the camera. The platform was moved by a diver along 2 parallel long rails placed across the excavation site. Additional, oblique photographs were taken along the sides of the ship and its keel line. Both techniques provided very good and accurate results (Drap, et al., 2007), (Zuchovsky, et al., 2013).

In offshore oil and gas industry, photogrammetry can be used both in underwater measurements of smaller-object like flanges, nodes and tees and more extensive surveys. Underwater photogrammetry was successfully used by Halliburton/BP Company in the Valhall Project. This project is the first long-route underwater survey which determined the position of a new platform. The result turned out to be very accurate and allowed to detected deviation from the asbuilt drawings (Johannessen & Prytz, 2005).

The greatest survey that used underwater photogrammetry was exploration of the Titanic. In 2010 the Woods Hole Oceanographic Institution expedition acquire detailed optical and sonar photographs of the Titanic using a Remotely Operated Vehicle and two Autonomous Underwater Vehicles. The result of the expedition was a high resolution ortophotomosaics and 3D model of the shipwreck (figure 7) (Behance, 2014).

Figure 7 *Underwater 3D model of the Titanic (AIVL, Woods Hole Oceanographic Institut, 2012)*

2.3 Underwater camera calibration

Camera calibration is a process in which parameters of interior orientation are determined: principal distance (camera constant), image coordinates of the principal point, lens distortions (radial and tangential) and affinity and shear. Radial distortion causes the major imaging error in the camera and it must be corrected. This distortion depends on lens design, focusing distance, object distance at a constant focus. Tangential distortion is caused by decentring and misalignment of the physical elements in lens. Affinity and shear components do not have impact on modern digital cameras and can be ignored. In order to acquire high quality 3D model, the images must be corrected. Lens distortion deforms the photograph and affects the geometry of the output model. The camera calibration process should be carried out before every measurement with a fixed focal length because every change of the focal length result in a change of the interior parameters.

The camera calibration process is based on a perspective geometrical model and bundle adjustment process. The calibration parameters are calculated based on the collinearity equation which is extended by the correction terms for the interior orientation and radial and tangential lens distortion. The model requires at least 5 corresponding points on a several photographs. This method determines all calibration parameters along with their precision and reliability. In the camera calibration process the 3D calibration grid is preferred from the plane calibration sheet. In addition the object should be covered by both horizontal and rotated photographs (Luhmann, et al., 2006), (Remondino, 2006), (PhotoModeler Help Topics, 2013).

The Brown calibration method is based on the assumption that straight lines in the object space must remain straight lines on the image when projected through a perfect lens. Any variation from straightness is attributed to radial or decentring (tangential) distortion and a least square adjustment is performed to determine the distortion parameters (Fryer, 1986).

The Brown distortion model describes 8 – term physical camera distortion parameters: principal distance, principal point offset, three coefficients of radial distortion: k_1, k_2 and k_3 and two coefficients of tangential distortion p_1 and p_2. Brown decomposed the total distortions into two components in polar coordinates on the imaging plane – along the radius and in tangential direction to the circle with the optical centre at the original point (before the distortion). The Brown model can simulate both barrel and pincushion type of radial distortion as well as mixture of these two types called sometimes a moustache distortion (Nowakowski & Skarbek, 2013).

The joined Brown model for the compensation function has the form:

$$x'_u = x'_d + \delta x,$$
$$y'_u = y'_d + \delta y,$$

$$\delta x = x'_d(k_1 r_d^2 + k_2 r_d^4 + k_3 r_d^6 + \cdots)$$
$$+ [p_1(r_d^2 + 2x'^2_d) + 2p_2 x'_d y'_d](1 + p_3 r_d^2 + \cdots),$$
$$\delta y = y'_d(k_1 r_d^2 + k_2 r_d^4 + k_3 r_d^6 + \cdots)$$
$$+ [p_1(r_d^2 + 2y'^2_d) + 2p_2 x'_d y'_d](1 + p_3 r_d^2 + \cdots),$$

where for the optical centre (x_c, y_c) we get:

$$x'_d = x_d - x_c, \qquad x'_u = x_u - x_c,$$
$$y'_d = y_d - y_c, \qquad y'_u = y_u - y_c,$$

$$r_d = \sqrt{x'^2_d + y'^2_d},$$

x_d, y_d - image distorted coordinates of the point,
x_u, y_u - image undistorted coordinates of the point,
x'_d, y'_d – approximate image distorted coordinates of the point,
x'_u, y'_u - approximate image distorted coordinates of the point,
r_d - radial distance,
k_i - radial distortion parameters,
p_i - decentring coefficients

All the equations are taken from the "Analysis of Brown camera distortion model" scientific paper written by A. Nowakowski and W. Skarbek (Nowakowski & Skarbek, 2013).

Underwater camera calibration must consider both standard interior orientation parameters and disturbance caused by the effect of refraction at air-glass-water interface. There are two major methods used in underwater surveying. In the first case the camera-housing system are treated as a whole unique system. No additional parameters connected with a different media interface are modelled. The other method uses both regular interior camera parameters and parameters associated with the refraction at air-glass-water interface (Diamanti, et al., 2012).

All rays in the submerged camera are refracted twice: at the water-glass and the glass-air interface, before they enter the camera (figure 8). The rays passing through the water-glass-air media do not meet in one common centre of projection. Using the perspective camera model for underwater surveying leads to systematic errors. In addition the type of the camera housing has a great impact on the camera's ray in submerged cameras. There are two major types of underwater camera housings: flat and dome. Dome ports could eliminate refraction effects caused by glass interface however this condition is very hard to fulfil. Both camera and housing must be very accurately aligned and precisely manufactured. On the contrary flat ports are cheaper and easier to produce but they cause bigger refraction effects (Sedlazeck & Koch, 2011).
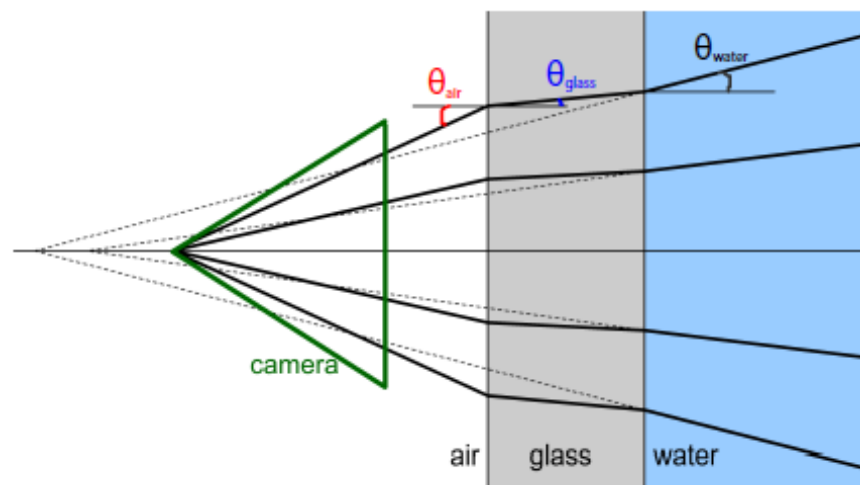
Figure 8 *Refraction at air-glass-water interface (Sedlazeck & Koch, 2011)*

Currently there is no available any professional software that can calculate the refraction due to water-glass-air interface. So, the unique camera-housing system are predominantly used in underwater surveying. If we assume that the camera housing is ideal (the glass port is perpendicular to the optical axis of the camera and all optical parts of the camera are symmetric along their optical axis) it turns out that the rays displace radially from the principal point. Summarizing the main part of the refraction due to the water-air interface

is radial. Obviously this assumption cannot be perfectly fulfilled in practice however it the large part the refraction error can be corrected using conventional camera calibration procedures. (Shortis & Harvey, 1998), (Drap, P., 2012), (Kwon, 1998).

The influence on the image plane by refraction due to the water-air interface is shown in figure 9. The object point *M* are projected on the image plane as point *I*. The interface plane refract the beam, thus the ray goes through the point R' instead of R. Point I' is the non-refracted image point and the space between I and I' is the error caused by refraction.
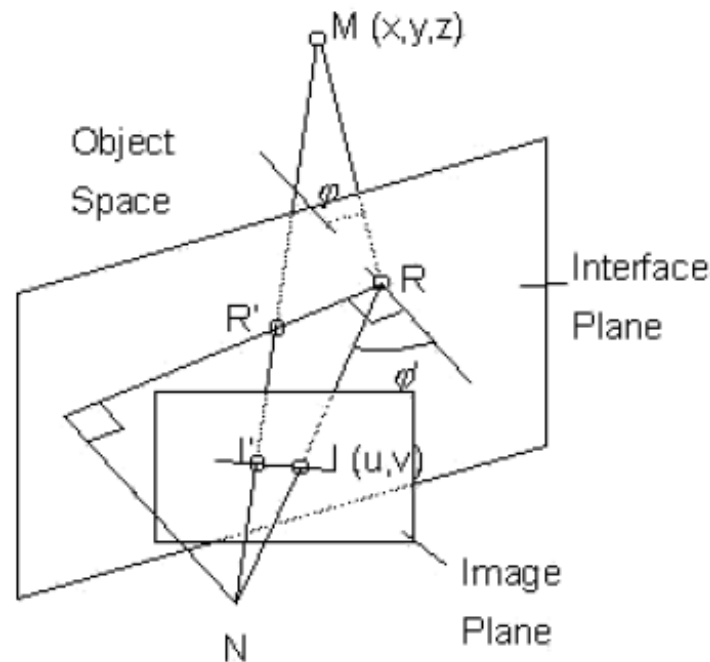
Figure 9 *Refraction at the water-air interface (Kwon, 1998)*

The refractive index is calculated based on the Snell's Law: Refractive index r is a ratio between the sinus function of the emergent angle **ф'** and the sinus function of the incident angle **ф**. For the water – air interface the refractive index is approximately 1,333.

$$r = \frac{sin\,\varphi'}{sin\,\varphi}$$

While the camera is in the air, the refractive index is equal 1 and the focal length is f. On the contrary when the camera is submerged the focal length value increase proportionally to the water refractive index. In consequence change of the focal length entails a high decrease of the field of view (figure 10). The underwater image looks wider than it is in reality because the emergent angle is larger than the incident angle. In a flat type of camera housing the underwater image shows deformation similar to pin-cushion distortion due to

the fact that the projection point *M*, point on the interface plane *R* and the perspective centre of camera *N* are not collinear (Kwon, 1998), (Lavest, et al., 2003).
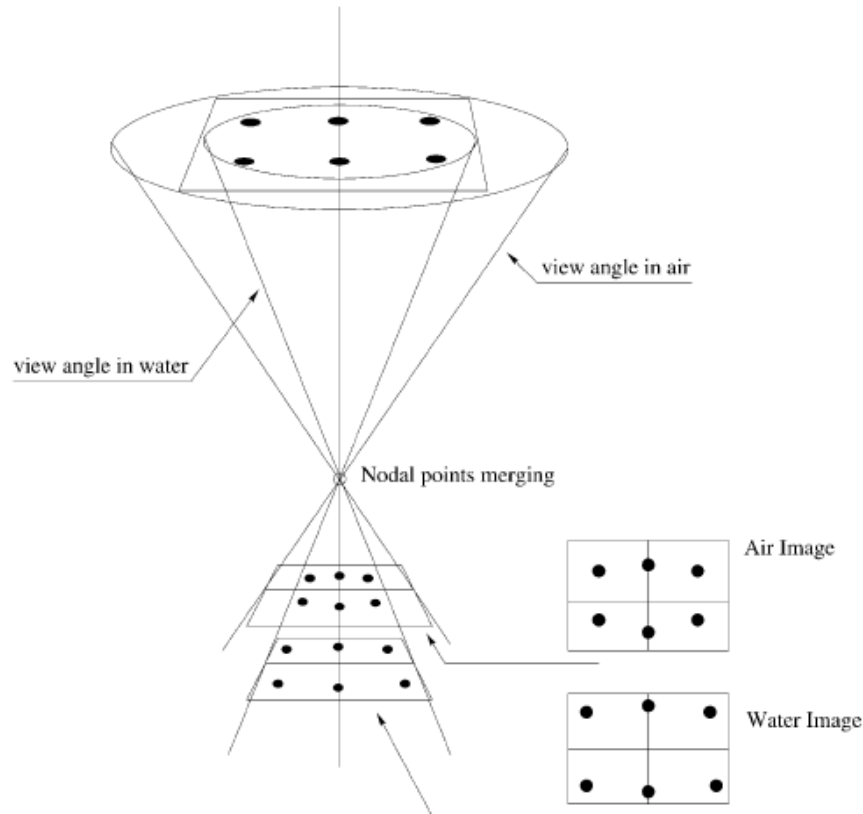
Figure 10 *Variation of the field of view between air and water (Lavest, et al., 2003)*

The camera should be calibrated in the same water medium that will be used in further measurements due to fact that the refractive index r can change with the depth, temperature and salinity of the water. The shape of the camera housing can change along with a change of pressure under the water and influence the interior parameters of the camera (Harveya, et al., 2003), (Shortis, et al., 2007).

At present a lot of research are conducted to deal with the refraction due to air-glass-water interface. Anne Sedlazeck and Reinhard Koch (2011) propose the refractive calibration method based on two stereo images captured using the stereo rig. In this method parameters connected with a different media interface are modelled. Beside regular camera calibration parameters, the normals of the interface surface with respect to the optical axis are used in this process (Sedlazeck & Koch, 2011).

Gili Telem and Sagi Filin (2010) suggested a two phase camera calibration based on the collinearity equation. The first step called "dry" estimates the standard intrinsic calibration parameters. The second step "wet", estimates the other parameters connected with the air-glass-water interface: refraction index, deviation of the optical axis from the interface and the distance between the perspective centre and housing port (Telem & Filin, 2010).

Anne Jordt-Sedlazeck and Reinhard Koch (2012) in the scientific paper "Refractive calibration of underwater cameras" propose calibration method based on both the geometric and radiometric parameters. Beside the traditional camera calibration procedure, the radiometric components are computed. This unusual solution allows to easily correct and enhance colours of the underwater images that afterwards can be used to colour correction of texture of the mosaic or the model (Jordt-Sedlazeck & Koch, 2012).

2.4 Calibration of the underwater stereo-camera system

The aim of the calibration of the stereo-camera system is an estimation of the position of the left camera relative to the right one. The calibration consists of two steps: relative orientation and absolute orientation. Relative orientation defines the separation of the perspective centres of the lenses (baseline), the pointing angles of the optical axes of the cameras and the roll rotations of the image sensors. External orientation determine cameras' position in the object coordinate system (Shortis & Harvey, 1998), (Luhmann, et al., 2006).
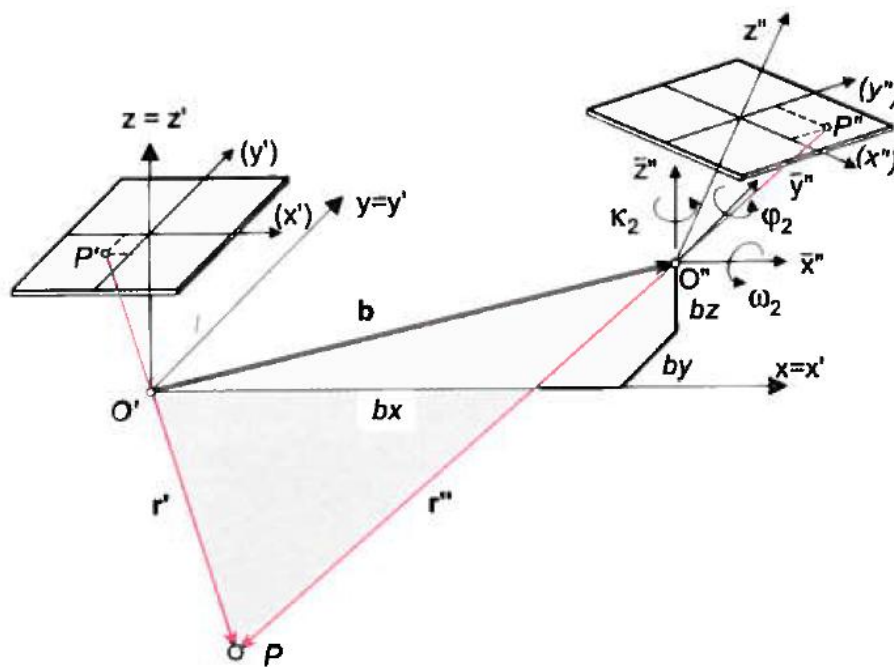
Figure 11 *Relative orientation (Luhmann, et al., 2006)*

The relative orientation is based on complanarity constraint which states that object point P and two perspective centres of both cameras O' and O" must lay in the same plane (figure 11). The local model coordinate system is fixed to the perspective centre O' of the left image. Thus, the exterior orientation (coordinates of the perspective centre and rotation angles) of the left image is set to 0. Usual the scale of the model is set to common value b_x

= 1. Then the parameters of the relative orientation consist of two base components: b_y, b_z, and three angles of rotation ω_z, φ_z, κ_z. The relative orientation parameters are calculated using the Least Squares Method (LSM) (Luhmann, et al., 2006), (Brager & Chong, 1999).

The epipolar plane is defined by three vectors b, r' and r'' and it contains the left image point P' and the right image point P'' (figure 11). The complanarity constraint requires that image rays going through both cameras must intersect (both rays r' and r'' must intersect in the object point P - there should be no y-parallax). The complanarity constraint is fulfilled if the scalar triple product of the three vectors b, r' and r'' are equal zero (Luhmann, et al., 2006).

$$(b \times r') \, r'' = 0$$

The stability of the stereo–camera system is subject to various conditions under the water. The changing pressure along with the water depth may affect the camera system and in consequence change the optical path to the lens of each camera. However as long as cameras are not removed from their housings, the system should remain stable. Thus, the same as interior orientation, relative orientations parameters should be estimated from data collected underwater (Havrey, et al., 2003).

2.5 Underwater light propagation

The poor quality of the underwater images are caused by limited range, insufficient and irregular illumination, colour absorption and low image contrast. Both proper illumination techniques on the site and image enhancement can improve the image quality.

The reflection of the light varies greatly depending on the structure of the sea. Incident light may bend from the water surface or reflect from it. Bended light result in crinkle patterns or diffusion (figure 12). Additionally the light may simultaneously partly reflect from the water surface and partly enter the water. The reflected light is both polarised horizontally and vertically. The vertical polarisation is very desirable in the underwater survey because it allows us to capture more colours then usual and the captured object is less reflective. (Iqbal, et al., 2007), (Knight, 2011).
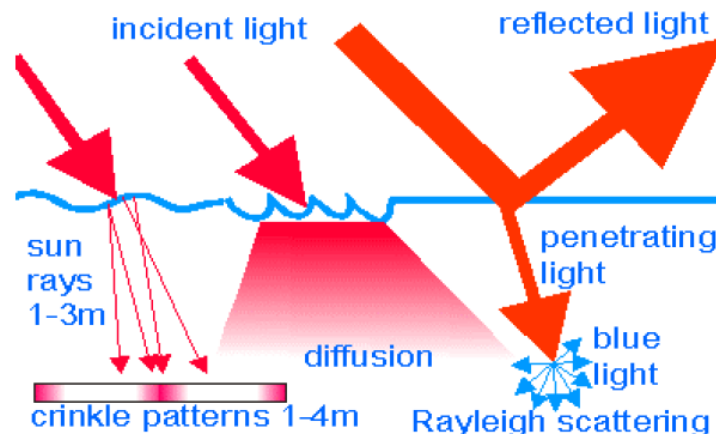
Figure 12 *Light effects on the water surface (Iqbal, et al., 2007)*

Underwater photographs may be affected by the backscatter and forward scatter phenomena which occur when light reflects from suspended particles or other underwater objects. Forward scatter appear when the angle of deflection is small and it results in image blurring and contrast reduction. Backscatter occurs when the light from the light source is reflected to the camera before reaching the object to be illuminated. Backscatter may cause bright points in the image (marine snow). The backscatter effect reduce significantly the contrast in the image and the marine snow make it impossible to process the data in the automated photogrammetric software. The influence of this phenomena increase with the distance between the camera and the object. The effect of this phenomena is shown in the figure 13 (Bonin, et al., 2011).
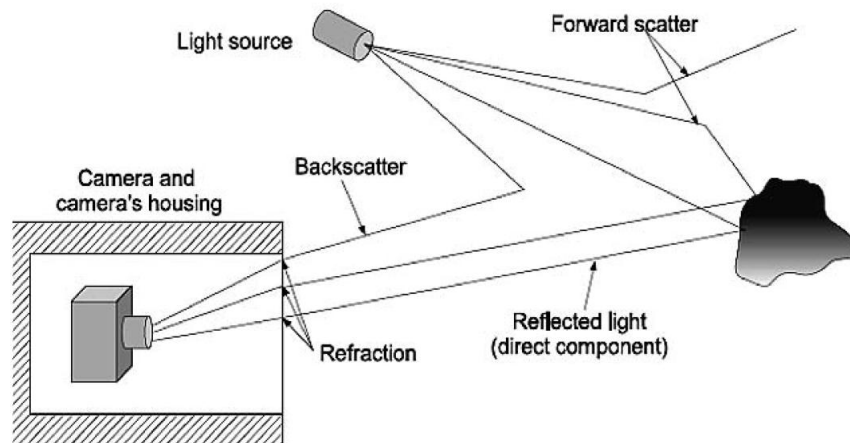
Figure 13 *Example of backscatter, forward scatter and refraction (Bonin, et al., 2011)*

Water absorbs light across the whole of the visible spectrum and the amount of light reduces with depth of water. The artificial lighting is often necessary in the deep water measurements. Moreover colours disappear depending on the wavelength length due to fact that water absorbs colour. The longer colour wavelengths is the faster colours disappears under the water. Therefore the red colour disappears first at the depth of 3

19

meters. Subsequently orange and yellow colour disappear accordingly at depth of 5 and 10 meters. Next green and purple colour will go off. The blue colour will disappear the last of all colours. Blue or green shade of the underwater pictures are caused by this phenomena (Iqbal, et al., 2007).

2.6 Underwater image enhancement

At present two main techniques are used in image pre-processing: an image restoration technique and an image enhancement technique. Image restoration technique requires additional parameters such as the attenuation and scattering coefficients and the distance between the camera and the object to correct the image. Image enhancement methods do not require any a priori knowledge of the environment and it may be performed in the widely available processing software such as GIMP or Photoshop (Drap, et al., 2011).

Underwater visibility and object structure can be recovered by polarization analysis. Aim of this approach it to eliminate the main degradation effects that are associated with partial polarization of light. Yoav Y. Schechner and Nir Karpel (2005) prepared algorithm which inverts the image formation process in order to enhance the quality of underwater images. This method can be efficient in shallow water where the underwater object can be illuminated by natural light. Additionally polarization filters decreases the amount of incident light to the lens that will result in a dark image. Use of a polarization filter is not efficient enough in deep underwater imagery. The comparison between the original and enhanced photograph by this technique is shown in figure 14 (Karpel & Schlechner, 2005).
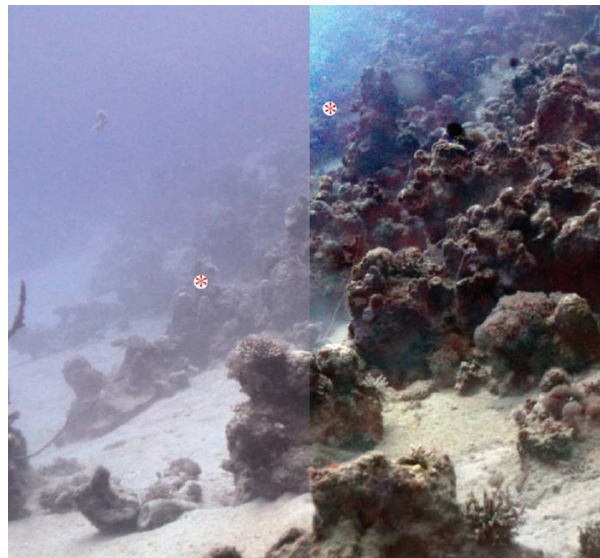
Figure 14 *Comparison between the original and enhanced photograph (Karpel & Schlechner, 2005)*

Another approach presented by K. Iqbal is based on slide stretching. The method is divided into two parts. Firstly, all the processes are conducted on the RGB colour model. The colour contrast of the image is equalized by histogram stretching. Subsequently the

saturation and intensity stretching on HSI colour model are performed. In consequence the image brightness is increased solving the problem of lighting. The photographs before and after performed enhancement by integrated colour method are shown in figure 15 (Iqbal, et al., 2007).

Figure 15 *Photographs before and after using an Integrated Colour Model* (Iqbal, et al., 2007)

Alessandro Rizzi and Carlo Gatta (2004) introduced the Automatic Colour Equalization ACE algorithm that can be used to correct underwater images. This method is able to reconstruct images with a highly variable lighting conditions. Moreover this algorithm allow to extract visual information from the underwater surroundings. The photographs before and after performed enhancement by ACE method are shown in figure 16 (Chambah, et al., 2004).

Figure 16 *Photographs before and after the enhancement by ACE method (Chambah, et al., 2004)*

3. System design

3.1 Vessel and Remotely Operated Vehicle (ROV)

R/V Gunnerus vessel

The research vessel was built in 2006 by Larnes Mekaniske Verksted in Norway (figure 15). The length of the vessel is over 30 meters and it is equipped in a few laboratories: wet lab, dry lab and computer lab. The the control container and the proper deck space allow to perform any measurements involving the ROV. The DP control system used on R/V Gunnerus vessel allows us to automatically control the position of the ROV in both local and external coordinate systems (Ludvigsen, 2010).

Figure 17 R/V Gunnerus NTNU research vessel (NTNU, 2014)

ROV Minerva

The Remotely Operated Vehicle (ROV) Minerva was designed in 2003 by Sperre AS. The dimensions of the ROV are 140 by 80 by 81 cm and it can work down to a depth of 700 meters. This vehicle can work efficiently at all depths in the Trondheimsfjord. The ROV Minerva can be used in marine biology research, deep water archaeology, offshore maintenance repair or marine monitoring and mapping. The vehicle is equipped with three CCD cameras, two manipulator arms, a scanning sonar, an altimeter and a HiPAP system used for the precise positioning. The most important feature is the very precise DP control system which allow us to manoeuvre the ROV automatically. This system can be applied to detailed photogrammetric surveys (NTNU, 2014), (Ludvigsen, et al., 2013). The ROV Minerva with basic equipment is shown in figure 18.

Figure 18 *ROV Minerva*

3.2 Underwater navigation

There are two main methods used in the underwater survey: the LBL (Long BaseLine) and the USBL (Ultra Short BaseLine) systems. The long baseline system (LBS) is an acoustic system based on the range measurement from at least 3 transponders mounted on the seabed. An interrogator which is mounted on the ROV transmits an acoustic signal to the transponders. Next the transponder send a response back to the system and the data is delivered to the system (figure 19). The position of the ROV is calculated using the Least Squares Method (LSM). This system can achieve a position accuracy below 1 meter. However if a few conditions are fulfilled such as an ideal geometry of the network, large distances between the transporters or when the LBL system operates without an acoustic path to the sea surface, the achieved accuracy can be around 1 cm (APOMAB, 1999).
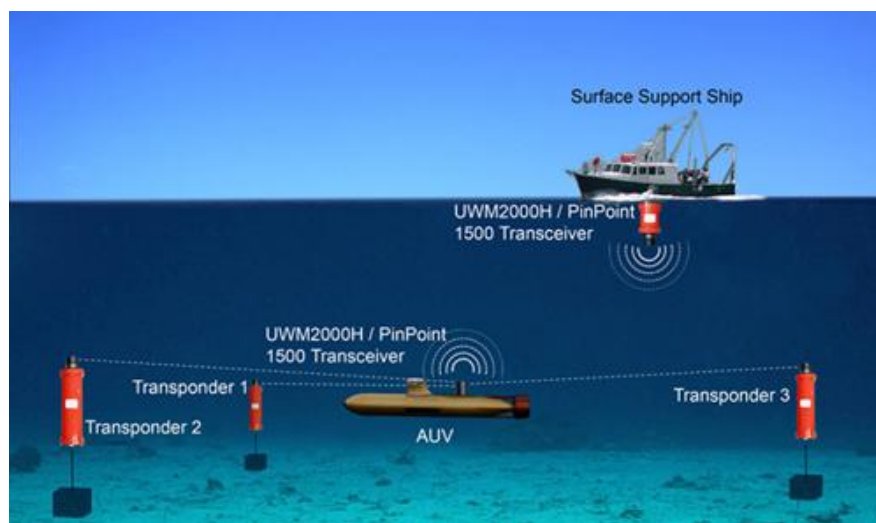
Figure 19 *LBL Acoustic Positioning System (AUVAC, 2014)*

The Ultra Short BaseLine (USBL) system consist of a transducer pole mounted on the ROV and transmitter on the vessel (figure 20). Additional sensors such as GPS, gyro, electronic compass and a vertical reference unit can be used to compute the pitch, roll and bearing of the ROV. The USBL system uses both angles and ranges to compute a position of the ROV. The range between the transducer and the transmitter is calculated based on an acoustic signal time. The angle is determined by a phase shift. The advantage of this system is that no transponders has to be mounted on the seabed. The accuracy of the USBL system depends on the distance between the transducer and the receiver and the quality of the sensor (APOMAB, 1999). The USBL system is shown in figure 20.
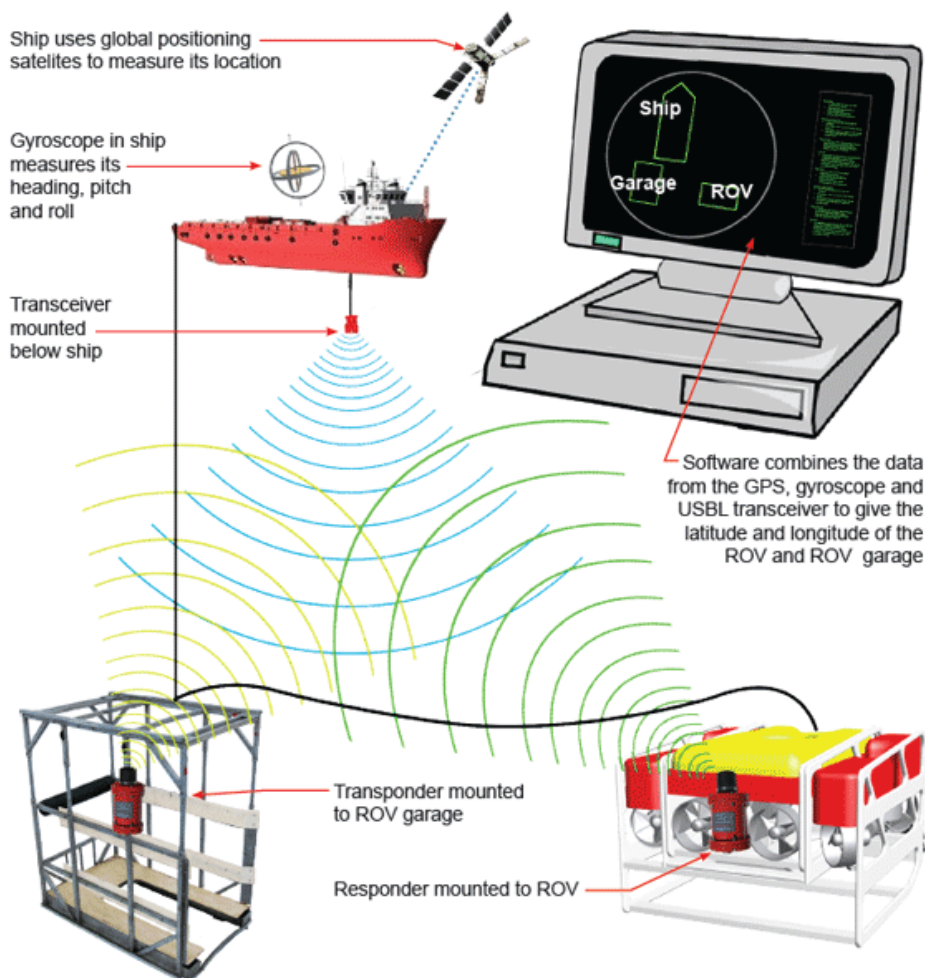
Figure 20 *USBL System (Systems, 2014)*

The position of the ROV related to the R/V Gunnerus is computed by the High Precision Acoustic Positioning System (HiPAP 500) which combines the advantages of the both the USBL and the LBL systems. This system requires only the transducer and one subsea transponder.

The Dynamic Positioning Control Platform (DP)

The ROV Minerva may be controlled both manually and automatically. However manual piloting is very inaccurate and ineffective. The Dynamic Positioning Control Platform (DP) was developed on NTNU in order to enhance the accuracy of the ROV's positioning and tracking. This system successfully keeps the position and designed trajectory of the ROV. The ROV controlled by the DP system keeps stationary and track lines below 10 cm with respect to the references. This system is extremely useful in underwater photogrammetric surveys. High control of the flight path is necessary when a certain overlap between the images must be achieved. The high variation from the designed track may result in a weak coverage of the object and, in consequence a failure in the further 3D modelling process. The system is described in detail in "Dynamic Positioning System for a Small Size ROV with Experimental Results" scientific paper (Dunkan, et al., 2011), (NTNU, 2014), (Ludvigsen, et al., 2013).

## 3.3 Stereo system unit

The stereo system unit consists of two cameras, two camera housings and a stereo bar mounted on a pan/tilt unit. The camera housings will be fixed to the stereo bar on the two holders by tie wraps. The position of the holders can be set arbitrarily on the stereo bar. The stereo unit is designed considering both the size of the camera and the available space on the ROV. In order to optimize the size of the unit both the chosen camera housings and the cameras are relatively small

Cameras

Work in a dark environment requires to use highly light sensitive cameras that increase the viewing range under water. Additionally these unfavourable conditions under water result in a low image sensor signal and in consequence noisy images. The camera should be equipped with a high size image sensor which increases light sensitivity of the camera (Ludvigsen, 2010). The camera must remain stable during the whole measurement. The intrinsic parameters should not change and the focus and the aperture number must be thoroughly fixed. Furthermore due to limited space on the ROV the cameras and the camera housings must be respectively small.

The chosen Prosilica GC1380C CCD 1.4 Megapixel industrial block camera (figure 21). The cell size of the camera is 6.45 µm. Body dimensions are extremely small and equals 59 mm x 46 mm x 33 mm. The GC1380 is equipped with the Sony ICX285 CCD Progressive type 2/3 sensor. The GC1380 provides low noise and high quality 1360 x 1024 resolution images (Allied Vision Technologies, 2013).

The camera is equipped with the high-resolution Cinegon 1.4/8 lens. The lens is very stable and insensitive to any vibrations which makes its suitable for underwater surveys. Focal length is 8.2 mm and image circle is 11 mm. F-number is adjustable and its range is 1.4 – 8. The wide camera aperture prevents blurriness on the images caused by ROV movements. The focus and Iris settings of the camera can be locked which provide the stability of the intrinsic parameters during the measurement. The camera has two ports: the gigabit ethernet port and the general purpose I/O port. The ethernet port transfers collected data to a computer. The I/O port provides power supply and other functions that allows the camera to synchronize with other devices (Kreuznach, 2014).

Camera housing

In the stereo vision system two stainless steel camera housings are used. Due to the fact that two different housing will be used, the position of the both cameras in the housings were adjusted to be approximately at the same distance from the port glass. In the first, larger camera housing (number 1 in the figure 22) additional holes had to be drilled in order to fix the camera. The position of the other camera in its housing was adjusted and fixed with respect to the position of the first camera.

Figure 22 *Camera housings*

The pin-outs of every electrical connector between the camera and the camera housing and the camera housing and the ROV were measured by a voltmeter to check the electrical circuit between them. Each contact of the connector had to be compatible with the corresponding connector in order to avoid damage or an incorrect connection between them. The preliminary settings of the pin-outs of the cameras were compatible with pin-outs of the camera housings. Next the ROV's male connector from the second, small camera housing were adapted to the new 10 pin port female connector used in the ROV.

Cameras were connected by the ethernet cable and the power cable to the camera housings. The ethernet cable transmits the video and photo data gathered during the measurement. The power cable provides the required power to the camera and allows us to communicate between the camera with the other, external system. The inside of the camera housing with fixed camera and connection cables is shown in the figure 23.

Figure 23 *Inside of the second camera housing with connection cables*

Stereo unit

The stereo unit consists of the pan/tilt unit, the stainless metal bar and two metal holders. The positions of the camera housings can be easily fixed and adjusted on the bar. The stereo unit allows us to remotely orient the stereo camera system in horizontal and vertical direction by an external system located on the vessel. The pan/tilt unit is shown in figure 24.
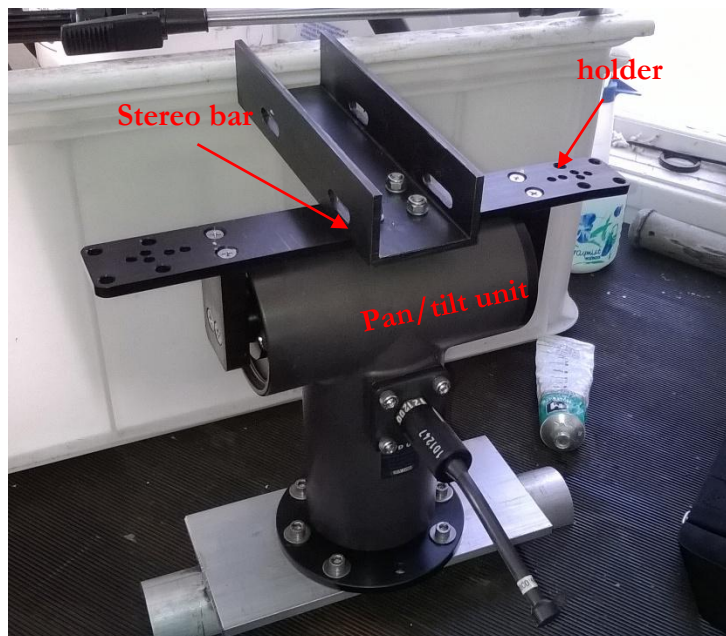

Figure 24 *The stereo pan/tilt unit*

The length of the original stereo bar was too small for this survey. In order to achieve good base-to-height ratio and decrease error on depths, a longer stereo bar had to be constructed and fixed on the pan/tilt unit. The newly constructed stereo bar with the camera housings fixed by stainless tie wraps on the holders is shown in figure 25.

Figure 25 *The camera housings n the new stereo bar*

3.4 Light source

The light disappears very fast under water with increasing depth. Artificial light is often necessary in order to illuminate the site during the underwater surveys. There are three main light sources used in the underwater survey: standard visible light sources which emit the light simultaneously, lasers and strobe or pulse lasers. It is recommended to use more than one light to illuminate the scene. The single light source produces a central bright spot surrounded by a poorly illuminated area. In the underwater measurements it is common to use different, stationary, light sources, especially if they emit a structured light. The light intensity cannot be too high so the details on the image can be distinguished easily. The advantage of the artificial lights is a reduction of the blurriness in the photographs. Mostly a big aperture size is used for shooting photographs under water so the additional illumination will allow us to decrease the exposure time. For photogrammetric purposes the underwater site should be illuminated evenly. A uniform illumination is required during the automatic photogrammetric process. Various lighting conditions between the photos may result in a failure of the automatic feature matching in the software. On the other site the artificial illumination results in shadows on the side that may cause problems in the automatic processing. If it is possible artificial light sources should be avoided during the photogrammetric survey (Bonin, et al., 2011), (Ludvigsen, 2010).

In this project due to a very dark environment (the depth of the shipwreck is over 60 m) it is required to use additional lighting. During the measurement four 250 Watts halogen lights and two 400 Watts HID lights mounted symmetrically on the top of the ROV will be used. The biggest advantage of HID lamps is the higher light emission in a spectral band where seawater have normally low absorption. The halogen light emits stronger rays in the red band of the spectrum and in result the red colour do not vanish that fast. This arrangement

should provide full illumination of the field of view of the stereo vision cameras under the water (Bonin, et al., 2011).

4. Methods and measurement

In this chapter the data acquisition and the camera calibration plan will be described. The type and size of the calibration sheet and the image shooting plan of the calibration sheet will be presented. Next the expected values of the focal length and the Field of View of the submerged cameras will be calculated. Based on the determined values, image acquisition plan with the number of strips and the exposure positions will be prepared. Furthermore the image processing method will be presented. The proposed image enhancement script will be explained and results will be presented. The examples of the original underwater images and the corrected underwater images will be compared. Finally the performed measurement and occurred problems will be described.

4.1 Data acquisition plan

Camera calibration

The aim of the camera calibration is to compute the interior parameters of the camera. A few calibration tests will be performed in different environments: in the air, in the freshwater and in the saltwater. Every calibration process should entail capturing around 30–40 photographs of a calibration sheet. The calibration sheet will be photographed from 4 sides parallel to the edges of the sheet. Both horizontal and rotated images will be taken and the images should cover the entire calibration sheet. At first, a test in the air will be conducted without the camera housings. The cameras will be fixed on the aluminium bar and set on the tripod. The checkerboard will be printed on an A0 format and taped evenly to the wall. The camera calibration procedure in freshwater and in saltwater will use a waterproof calibration sheet made from an aluminium plate with a printed checkerboard (squares size 8 cm). The size of the calibration sheet is 1.60 m x 1.25 m and it is heavy enough to submerge it into the water. The camera housings will be fixed to the stereo bar and the calibration photographs will be taken both in a test pool and site in the sea.

The historic shipwreck measurement plan

The survey will focus on the main part of the historical shipwreck. The examined area is 20 m x 2 m and it includes the keelson and the bow of the object (figure 23). Photographs will be taken by the two cameras fixed 45 cm apart from each other on a stereo bar. The two cameras with 8.2 mm focal length and an 8.77 mm x 6.60 mm (2/3') sensor format will be used. Both vertical and oblique photographs will be taken. The vertical photographs will cover the whole investigated area. The oblique photographs will cover distinctive objects rising up from the seabed. The fly path are prepared according to aerial photogrammetry foundations.

The photographs will be taken from a distance of 1.5 meter from the object. It is the shortest value where photographs may be taken without causing the ROV to interfere with the sandy seabed. Any interface with the seabed will disturb the particles and result in a lack of visibility. In this case the base-to-height ratio of the stereo pair will be 1: 3.33.

Three scale bars (one 4 meters long and two 2 meters long) will be placed on the seabed. A long one will be set up parallel and two other perpendicular to the shipwreck. The external orientation of every cameras' position will be computed from the DP system launched on the vessel.
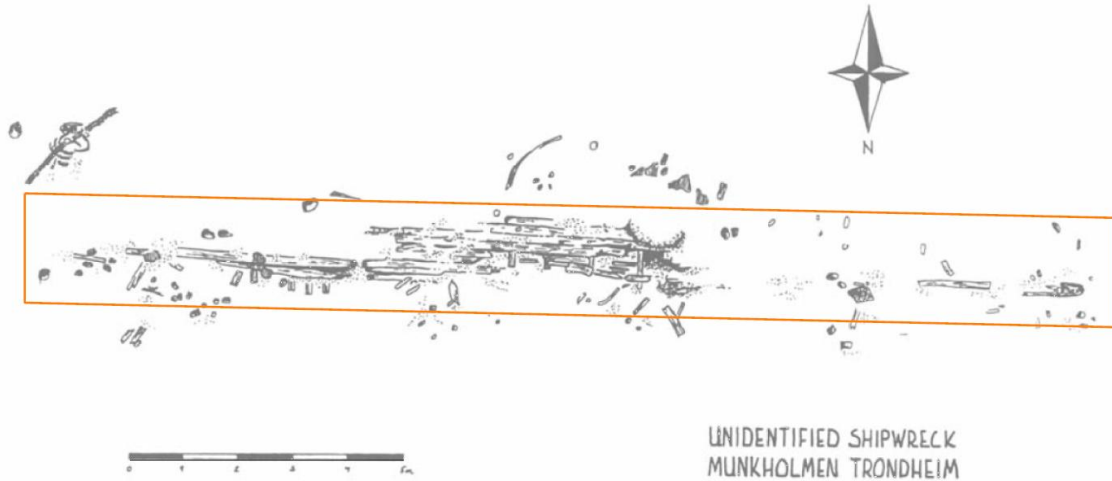
Figure 26 *The measurement area*

The expected focal length and field of view (FOV) under the water are calculated from the preliminary values given by the manufacturer of the camera (table 1). The refractive index in the salty water is assumed 1.339. The FOV in the air, FOV under the water and focal length under the water are computed from the below equations:

$$FOV_{Air} = 2\tan^{-1}\left(\frac{d}{2f}\right),$$

$$FOV_{Underwater} = 2\sin^{-1}\left(\frac{\sin\frac{FOV_{Air}}{2}}{r}\right),$$

$$f_{Underwater} = \frac{d}{2\tan\left(\frac{FOV_{Underwater}}{2}\right)},$$

Where:

FOV_{Air} – Field of View in the air,

$FOV_{Underwater}$ – Field of View under the water,

$f_{Underwater}$ – Focal length under the water,

d – Diameter of the image sensor,

r – Refractive index.

Table 1 *Preliminary and expected focal length and FOV.*

	Focal length [mm]	FOV diagonal [deg]
Preliminary values	8,2	67,6080
Computed values (expected values under the water)	11,65	49,1015

The further calculations are conducted based on the expected values. The submerged camera should cover 1129 mm x 850 mm area with a 0.83 mm terrain pixel size. The overlap between photographs taken from the two cameras on the stereo bar are 70% and the photographs covered by a stereo unit should overlap 20% (figure 27).
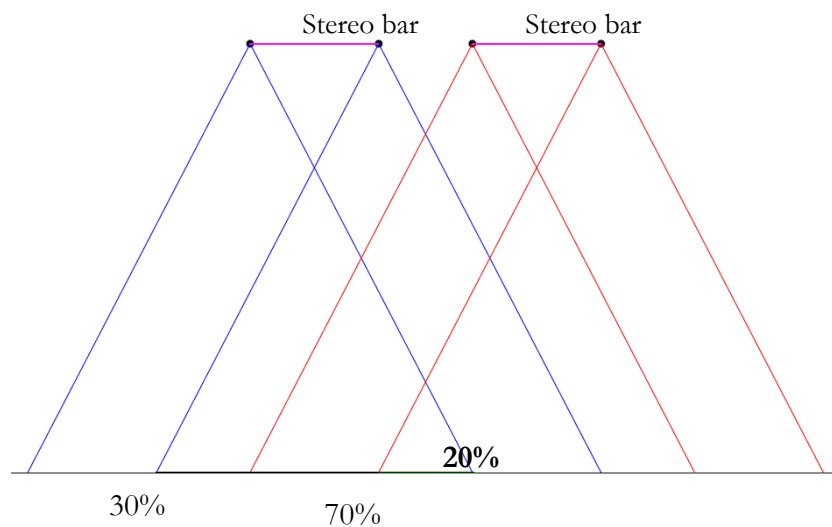
Figure 27 *Stereo overlap plan*

The lateral overlap between every strip should be at least 60%. The flight lines will be positioned along the boundaries of the designed area. Flight direction will be consistent with the historical shipwreck axis. The vertical photographs will be taken in 6 strips with 28 photographs on every strip (total 168 photos). The estimated position of the strips and the exposures is shown in figure 28. The final values will be calculated after investigation of the historical shipwreck by the ROV during the measurement.

Figure 28 *The data acquisition plan*

The bow and the middle part of the keelson will be covered by the oblique photographs. The proposed photographed area is shown in figure 29. However due to lack of data about

size of the individual objects, precise plan of a photographing of these areas will be decided on side.

Figure 29 *The historical shipwreck site with a highlighted, probably rising from the seabed parts.*

There are a few things that must be taken into consideration while taking underwater photographs: the illumination, the Depth of Field (DOF) and the speed of the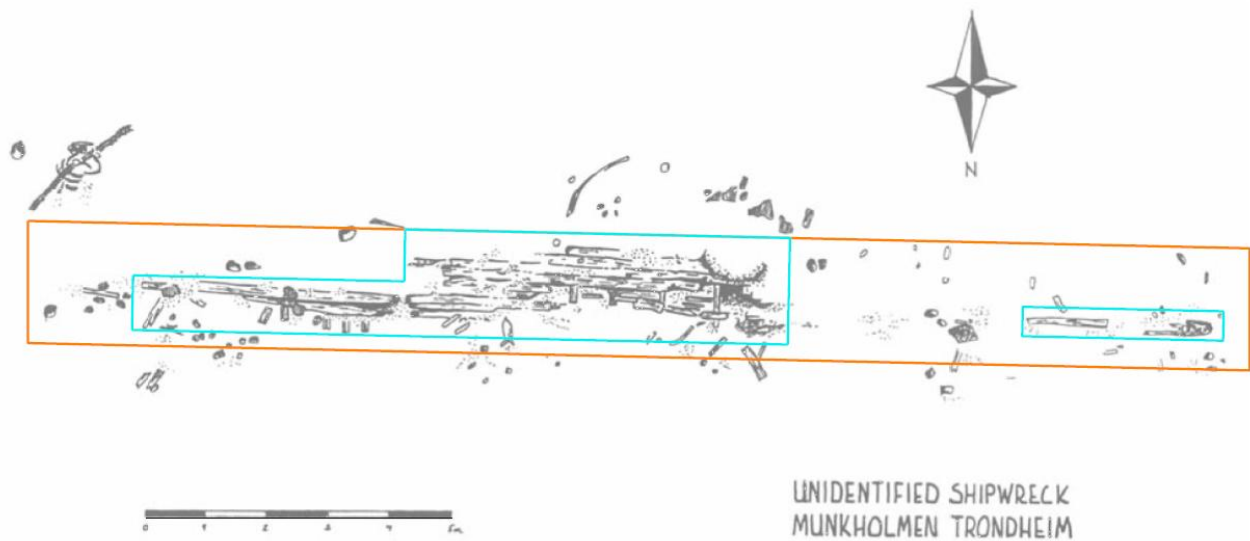 ROV. The aperture and the exposure time camera's parameters should be balanced. Due to poor illumination on the underwater site the aperture should be large enough to enter more light. On the contrary the big aperture decrease the DOF that results in a small distance in the scene where the object is sharp on the photograph. Additionally the exposure time should not be too long because the photographs will be taken by a moving ROV. If the ROV move fast, the photographs will be blurry.

In this survey the aperture of both lenses will be set to the smallest value 1.4 mm. The exposure time will be set to 1/40 or 1/50 sec and the ROV movement will be adjusted that the photographs will be still sharp. The ISO, brightness and White Balance (WB) parameters will be set on the site depending on the underwater environment.

4.2 Image processing

The aim of the underwater image processing is a restoration of colour, contrast and lighting in the images. Underwater images are blurred, murky and dominated by a blue colour and cannot be used efficiently without previous enhancement in the further image processing analysis. The proposed algorithm perform calculations on RGB, HSI and HSV colour maps. The initial processing on RGB model will balance red and green channels in comparison to blue channel. Next the HSI and HSV models will be used to enhance other variables: Saturation (S), Intensity (I) and Value (V). Saturation and intensity values generate

the wider colour range and allow us to strengthen the contrast ratio in the underwater images. The value 'V' is the largest component of a colour in HSV model and it defines the brightness of colours. The value allows to brighten the image and helps distinguish details in the image (Iqbal, et al., 2007).

The algorithm corrects images in three colour compositions: RGB, HSV and HSI. First RGB histogram percentage linear stretching is used to correct colours and equalize contrast of the image. The 1% of the upper and the bottom values of red, green and blue channel are specified. The old minimum values are matched to the new minimum values, and the old maximum values are matched to the new maximum values. Middle values are spread evenly between the new minimum and maximum values. Next 1% linear stretching are performed on saturation and value on HSV colour model in order to enhance lighting and improve true colour of the image. Finally intensity value are equalized by contrast-limited adaptive histogram equalization on HSI colour model to balance lighting and brighten the image.

The result of processing of the test images is shown in figure 30. It appears that proposed algorithm works successfully on the underwater photos. It both equalizes the colour contrast and brightens the image. Blue and green tones are reduced and contrast is increased what result in clear and readable images.

BEFORE **AFTER**

Figure 30 *Pictures before and after image correction.*

4.3 Measurement

The measurement of the historic shipwreck

First the ROV was submerged in order to investigate the underwater shipwreck. The all area of interest were carefully examined by the camera located on the underwater vehicle. The historic shipwreck is consistent with the previously seen maps and plans. A particular attention was paid to the protruding parts of the object in order to decide which elements must be covered additionally by the oblique imagery. In result of this investigation the bow and the middle part of the underwater object marked red on figure 31 were decided to be photographed by oblique images.
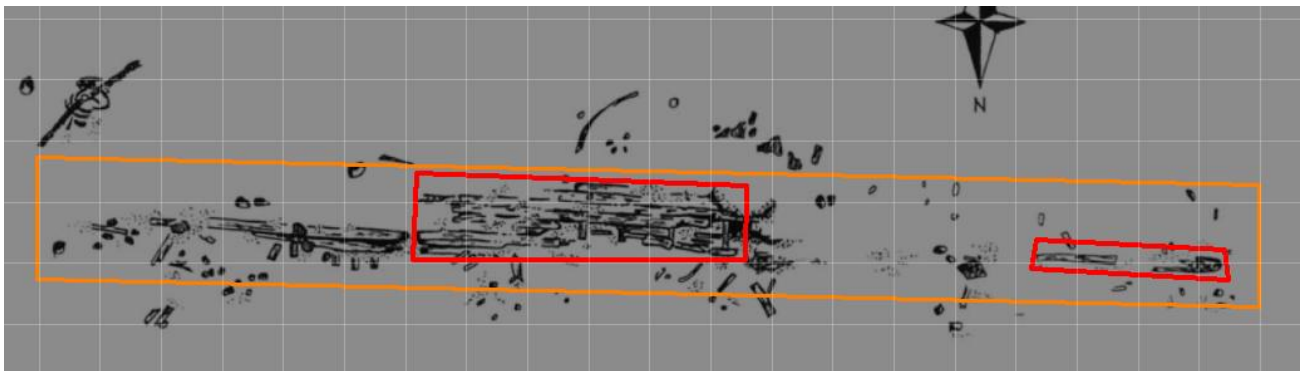

Figure 31 *Marked areas that will covered by the oblique photographs*

The water environment surrounding the underwater shipwreck was very clear. The water was not turbid so the visibility was extremely high. The amount of the particles in water were very low. No layer of sediment was settled on the object and the wooden parts were clearly visible. The seaweed occurred only on a few parts of the object. No other, significant obstacles occurred on the object that may influence the created model except a starfish on the wooden keelson.

As it is clearly seen in figure 32 the visibility decreases with the increasing distance from the object. The first and the second photographs are taken respectively from approximately 3 meters and 1 meter distance from the historical shipwreck. The bow on the second image is clearly visible without any big loss of colour. In consequence it can be assumed that the used light is sufficient to brighten up the area of interest and no additional adjustment need to be performed. Additionally as it was predicted, the artificial lighting resulted in the shadows on the underwater scene. However on this depth where no natural light occurs artificial lighting is necessary.
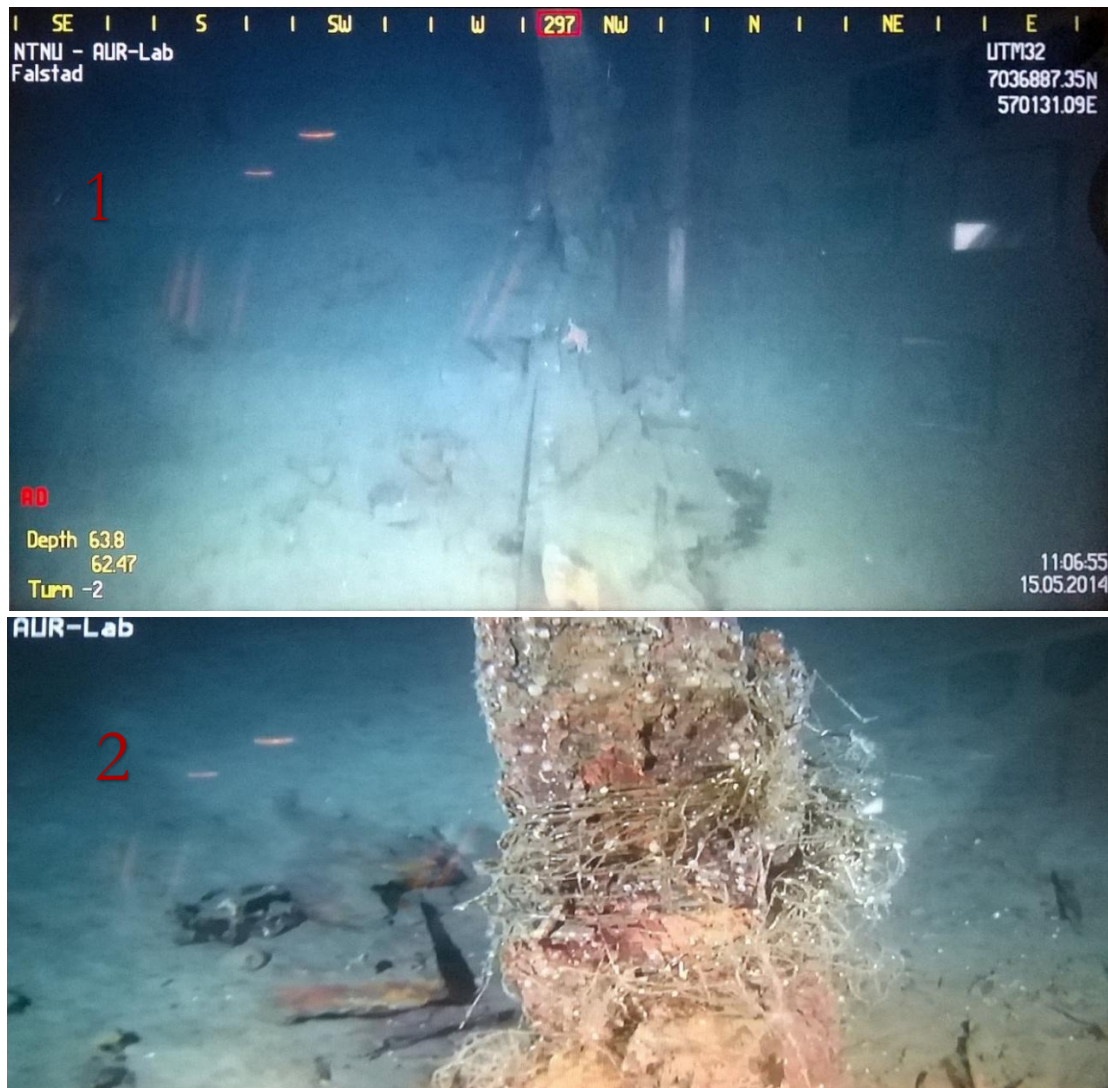
Figure 32 *The keelson (1) and the bow (2) captured by the ROV*

A few unexpected problems occurred during the measurement. First the software was supposed to take photographs from the both cameras simultaneously failed. Software did not recognize one of the cameras and consequently no surveys could have been performed until this problem was solved. The other problem was connected with the used equipment. One cable was rusted and it had to be replaced. Due to lack of the spare equipment, the cable must have been purchased. The cable did not come on time and the measurement had to be postponed. Finally it has been decided to perform test measurement offshore of the pipeline and the submerged object. The historical shipwreck will be measured in August 2014 and it will be a subject of scientific paper.

The measurement of the pipeline and the submerged object

On the beginning the cameras were connected to the computer and a few test were performed to check if software is working properly. The focus of the both cameras were tested once more and the exposure value were set to 1/50 second. Unfortunately the left

and the right camera did not take photographs simultaneously. The time between exposures differed by 0.1 second. In order to reduce the error due to this time difference, the ROV speed was decreased and set to 0.2 m/s. In that case the ROV will move 2 cm between the camera exposures. This value should not influence the automatic 3D model generation but it may interfere with the stereo calibration parameters. The positioning system failed due to equipment failure and in consequence no external position data was available.

The Pan/Tilt unit could not be connected to the computer so other equipment had to be used. The new unit was not able to move as freely or easily in every direction as the previous one so the stereo bar must had to be fixed in two positions on the ROV: in the front to take oblique photographs and on the side to take vertical photographs.

The camera housings were fixed on the stereo bar in a distance of 43 cm. The stereo bar was fastened securely on the ROV first on the front and then on the side of the vehicle in order to verify if it can easily fit on the vehicle (figure 33). The position of the lights were adjusted in order to illuminate the underwater site evenly. Furthermore the lights were turned on to check if any shadows is caused by the protruding parts of the vehicle. The range of the ROV is limited to 1000 metres due to the length of the cable.
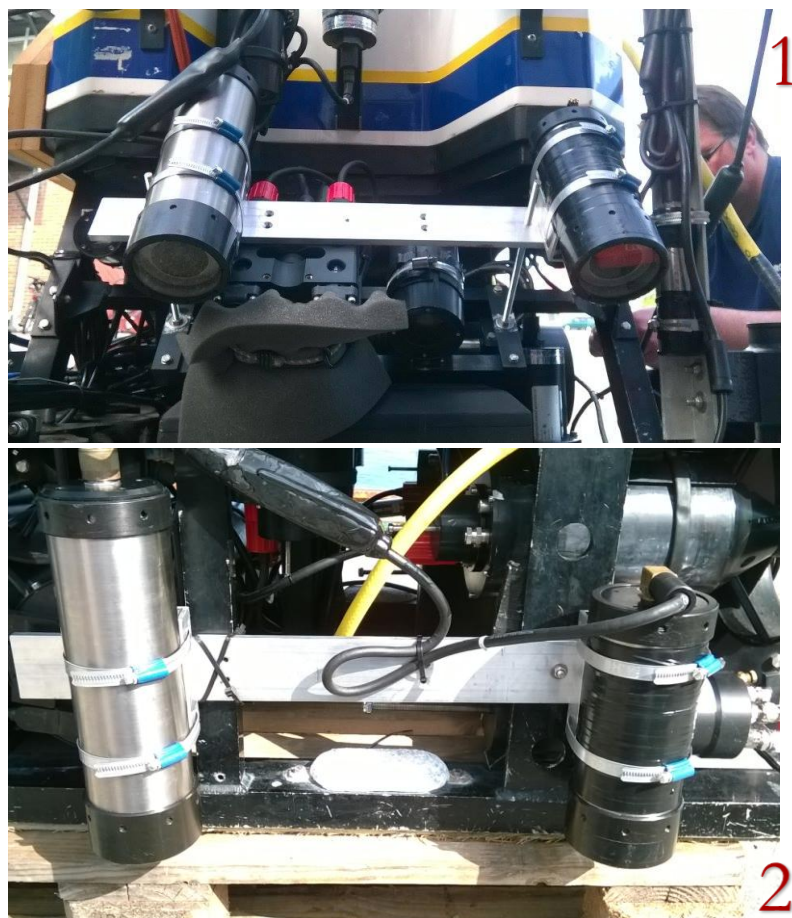

Figure 33 *The stereo bar fixed in the front (1) and on the side (2) of the ROV*

<u>The pipeline measurement</u>

In order to shoot the vertical photos the stereo bar was fixed on the side of the ROV. The vehicle together with the measuring rod carried by the manipulator arm were submerged. The underwater positioning system did not work so the area had to be searched in order to find the pipeline. The measuring rod was placed along the pipeline. The measurement will be conducted similarly to the previously prepared plans for the measurement of the historical shipwreck. All the necessary data was inputted into the DP control system. The area will be covered by three strips from a distance of 2 meters from seabed. The length of the strip was set to 20 meters and the distance between the two neighbouring strips were set to 40 cm. The photographs will be taken every 1 seconds and in result the distance between neighbouring exposures will be 20 cm. The additional data will be removed later in the post processing. The above settings were set accordingly to the calculated values from table 2. The flight plan was calculated assuming that the image width along flight direction is equal to the total length of the area covered simultaneously by the left and the right image.

Table 2 *Flight plan settings*

Area width [mm]		20000
Area height [mm]		1000
Image scale factor	H/c	223,10
Length overlap %	B	**40**
Sideway overlap %	S	**60**
GSD [mm]	GSD	1,11
Photo width [pix]	s_L	1360
Photo height [pix]	s_C	1024
Photo width in image space [mm]	w	8,772
Photo height in image space [mm]	h	6,605
Image width along flight direction [mm]	S_L	1980
Image height across flight direction [mm]	S_C	1134
Longitudinal overlap [mm]	p	792
Transversal overlap [mm]	q	680

The length of the baseline [mm]	B	1188
Baseline in the image space [mm]	b	5
The distance between two neighbouring flight lines [mm]	A	453
The covered model area [mm²]	F_m	1568160
Numbers of photo per strip		17
Strips per block		3
Total number of photos		51

Before the DP system was launched the vehicle had to be set along the pipeline. Without the positioning system the vehicle could not be aligned accurately along the object. Additionally the ROV was very shaky and it did not keep a stable position. As soon as the vehicle was set into the desired direction the DP control system was started. The vehicle got out of the set direction but it still covered the area of interest. The DP system worked very well even without data from the positioning system. The ROV moved according to the settings input to the system. During the measurement the software responsible for taking photographs crashed. A part of the first line and the second line were not covered by photographs and the whole process had to be repeated. The vehicle was set up again approximately in the same position and the DP control system was launched. However the connection between the ROV and the computer got lost and the vehicle had to be surfaced and brought offshore. Afterwards the vehicle was repaired but due to lack of time the pipeline could not be remeasured. In addition the scale bar had not been photographed during this run and in result no external data is available.

Camera calibration

Before any further measurements the stereo bar were mounted in the front of the vehicle in order to take oblique photographs. The calibration sheet was submerged from the shore using ropes. Around 160 photographs were taken simultaneously from both of the cameras. The three sides of the calibration sheet were photographed from different angles. No measurements were conducted from one of the sides of the calibration sheet due to limited space caused by the close proximity to the shore. All the photographs were taken without use of the artificial light due to very good visibility under water. No particular problems occurred during this process.

The underwater object

The neighbouring area were investigated in order to find a suitable underwater object. It has been decided that the submerged winter shovel would be measured. The object has sufficient size and it is placed not that far from the area where the camera calibration process was performed. The underwater object were covered by the photographs from all sides. Photographs were taken constantly at 2 seconds interval from different angles and distances from the object. The position of the ROV was navigated manually using a special control panel. The vehicle was moved based on a view from the video camera (figure 34). During the measurement the captured data was constantly checked. Again the software responsible for taking photographs crashed but due to a huge amount of taken photographs this did not affect the conducted project. Finally around 550 photographs of the object were taken simultaneously by the left and the right camera. No external data was obtained during this run.

Figure 34 *The measurement process of the underwater object*
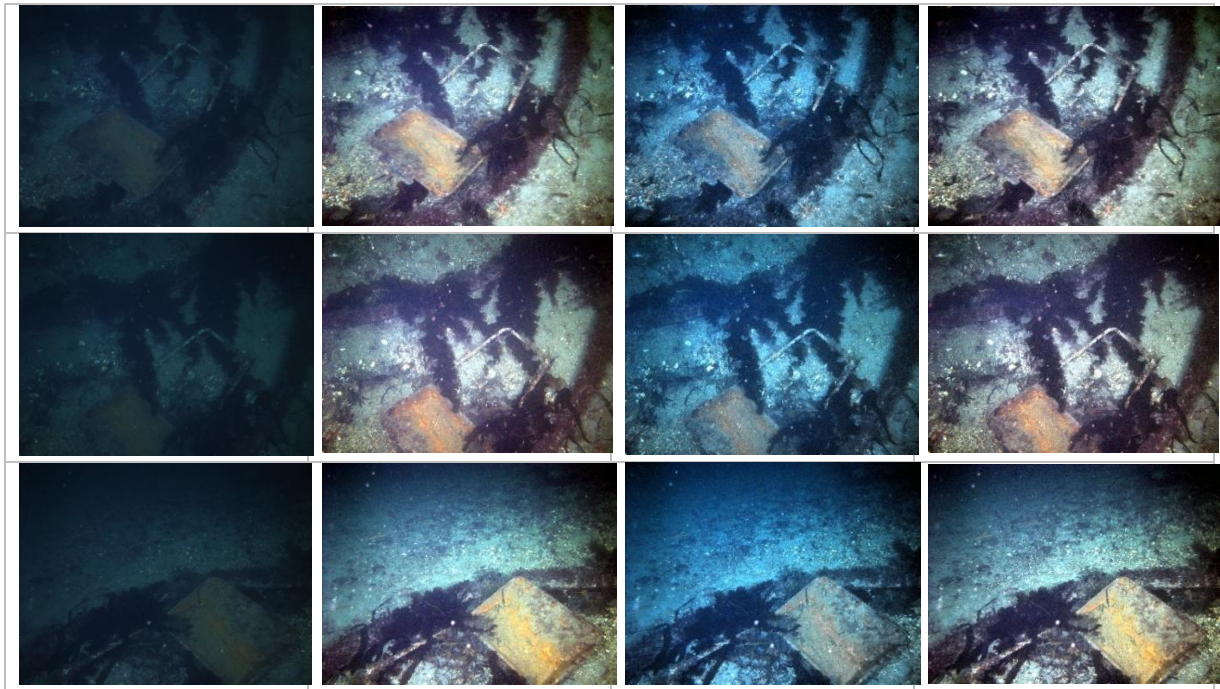
5. Data processing

5.1 Image enhancement

The underwater images were corrected using the previously proposed script described in 4.2 section. The aim of this process is an improvement of the quality of the underwater images and increased feature detection in further automatic processing. To this analysis 4 photographs taken from different angles and distances to the object were chosen. Original photographs were compared with three differently processed images with accordingly applied algorithms: histogram equalization on RGB model, Intensity, Saturation and Value correction on HSI and HSV colour models and with both previously mentioned adjustments. Colours in the original underwater photographs are muted and dominated by blue hue.

The images with performed contrast stretching on RGB model are brighter and well contrasted. The average colours in the images are equalized, thus blue colour does not dominate the whole scene. This algorithm works well when the object is photographed from the close distance (1-2 m). However noise and blurriness increase along with the distance from the object. The centre of the distant images is overexposed and dark colours are dominated by magenta tone. Colours are not similar to the true hue. Images with applied Intensity, Saturation and Value correction increase visibility on the photographs and enhance the true characteristic of the object. The processed images are sharper and clearer and features are well recognizable but blue colour is still dominant. The centre of the photographs are not that overexposed considering the previous correction. Finally the combination of these two methods results in both colour corrected and less blurred images. The middle of the photograph is still bright but in comparison to the previous algorithms the result is satisfactory. The colour is still not close to the real hue and the noise ratio is increased on the images photographed from larger distance from the object. Comparison results is shown in table 3.

Table 3 *Images corrected on the proposed model*

Original photograph	RGB correction	I, S and V correction	RGB and I, S and V correction

Additionally photographs were processed in Adobe Photoshop Lightroom 5.4 and the suggested algorithm. The three enhancement methods are proposed. First process were conducted only in Adobe Photoshop Lightroom. In this process automatic white balance was set and contrast and exposure values were increased. In addition shadows and whites details values were increased to brighten the dark areas. Saturation and luminance of yellow, green and blue were adjusted on the HSL colour model to enhance and restore the true colours. The colours in the processed images are still muted but they are closer to the natural colour then in the previous test. Next saturation, intensity and value enhancement of the previously corrected photographs using the proposed model were used. The individual features on the images become more visible however noise raised and yellow colour become dominant. In the last process automatic white balance was also performed. Additionally colour temperature was slightly decreased. Contrast and exposure values were increased and highlights and overall saturation were adjusted. Green and yellow colour were corrected on the HSL model. Colours are muted, however they are more natural than in the first and second case. Finally the first and the third colour correction model conducted in the Adobe Photoshop Lightroom will be used in the further automatic photogrammetric process. These methods provide the most similar results comparing to the natural colours. Although colours are muted it these will provide better result because of lower level of noise in the images. The high contrast and exposure values of the images results in reduced visibility and low feature recognition. Comparison results is shown in table 4.

Table 4 *Images corrected in Adobe Photoshop Lightroom and the proposed model*

Original photograph	Images corrected by *Lightroom* (1)	S, I and V correction	Images corrected by *Lightroom* (2)

5.2 Camera calibration process

The camera calibration process was performed in the two different software: AgiSoft Lens and Camera Calibration Toolbox for MatLab. In both software the radial and the tangential distortions are modelled using Brown's distortion model. The estimated interior camera parameters are the horizontal and vertical focal lengths, the coordinates of the principal point, the radial and tangential lens distortions and the skew coefficient. Both systems define the origin of the image coordinate system at the top left image pixel. The checkerboard calibration sheet is used for the processing in these software.

Camera calibration toolbox for MatLab is an open source code created by Jean-Yves Bouguet. The software is based on a method described in scientific paper "A Four-step Camera Calibration Procedure with Implicit Image Correction" where empirical inverse model is used to correct images. The empirical inverse model combine the pinhole model camera with the corrections for radial and tangential distortions. The Direct Linear

Transformation (DLT) and the non-linear least-square parameter estimator is used to estimate initial values for the camera parameters. The image correction is performed by an interpolation of the correct image points using the physical camera parameters calculated in the previous steps. This software can be used both with 2D calibration sheets and 3D calibration grids (Heikkilä & Silven, 1997).

Formulas used to calculate the interior parameters in both AgiSoft Lens and Camera Calibration Toolbox for MatLab are given in manuals available online and are listed below (Bouguet, 2013), (Lens, 2011):

$$x = \frac{X}{Z}$$

$$y = \frac{Y}{Z}$$

$$x' = x(1 + k_1 r^2 + k_2 r^4 + k_3 r^6) + p_2(r^2 + 2x^2) + 2P_1 xy$$
$$y' = y(1 + k_1 r^2 + k_2 r^4 + k_3 r^6) + p_1(r^2 + 2y^2) + 2P_2 xy$$

$$u = c_x + x' f_x + y' \cdot s$$
$$v = c_y + y' f_y$$

The unit conversion are computed using the following formula:

$$\begin{bmatrix} u \\ v \\ 1 \end{bmatrix} = KK \cdot \begin{bmatrix} x' \\ y' \\ 1 \end{bmatrix}$$

$$KK = \begin{bmatrix} f_x & f_x \cdot s & c_x \\ 0 & f_y & c_y \\ 0 & 0 & 1 \end{bmatrix}$$

Where:
$$r = \sqrt{x^2 + y^2}$$

X, Y, X - point coordinates in the local camera coordinate system,
u, v - projected point coordinates in the image coordinate system,
f_x, f_y – horizontal and vertical focal lengths,
c_x, c_y – coordinates of the principal point,
k_1, k_2, k_3 – radial lens distortions,
p_1, p_2 – tangential lens distortions,
s – skew coefficient.

The stereo camera calibration is performed in the "Camera Calibration toolbox for MatLab" software. The extrinsic parameters of the left camera are fixed and set to 0. The position of the right camera with respect to the left camera are defined by the rotation

vector and the translation vector. The model is scaled based on the size of the squares from the checkerboard.

In AgiSoft Lens the camera calibration process is conducted entirely automatically. No manual measurements of the checkerboard had to be performed. Different set of parameters can be chosen for calculations. The focal length must always be fixed, but cx, cy, k1, k2, k3, k4, p1, p2 and skew parameters can be chosen arbitrarily. The processes were performed using all parameters besides the k4. The software recommends to use photographs where the checkerboard fills up the entire view. However the calibration images do not fulfil this requirement, due to the fact that the camera calibration will be performed in two different software and Camera Calibration Toolbox for MatLab needs to cover the whole or the same part of the calibration sheet on every image, it has been decided to take photographs according to the recommendations given by Camera Calibration Toolbox for MatLab manual.

AgiSoft lens did not measure any points on the rotated photographs (figure 35). Probably the algorithm used in this software is less advanced and it cannot deal with the differently rotated images.

Figure 35 *The horizontal and the rotated image with the measured image points in the AgiSoft Lens.*

In Camera Calibration Toolbox for MatLab the grid corners need to be extracted manually on the each photograph. This software is more advanced than AgiSoft Lens and it allows us to set various parameters during the calibration procedure. The Toolbox can compute the interior camera parameters using different calibration grids (planar 2D sheets or 3D calibration grids). Furthermore the parameters of the stereo calibration can be calculated.

In this camera calibration process, a length of the squares on the checkerboard plate was inputted into the software to scale the stereo calibration parameters to the actual values. The grid corners had to be marked starting from the same corner in the clockwise direction otherwise the software will not compute the result correctly. The image points with errors measured in Camera Calibration Toolbox for MatLab is shown in figure 36.
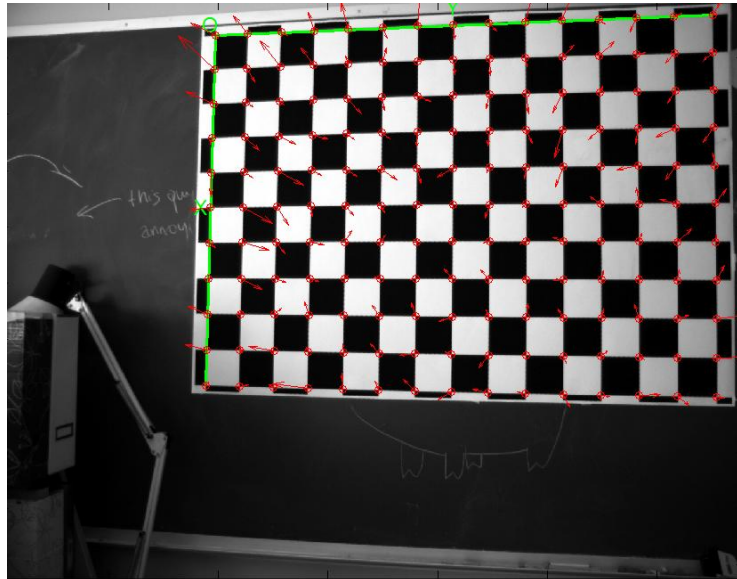
Figure 36 *The image points with errors measured in the Camera Calibration Toolbox for MatLab.*

The camera calibration performed in the air

Computed focal lengths of the left and right camera do not differ much from the preliminary value 8.2 mm provided by the manufacturer. The focal lengths, the coordinates of the principal points and the radial distortions k_1 and k_2 calculated respectively for the right camera and the left camera by both software are almost the same. On the other hand, the rest of the parameters differ significantly from each other. The accuracy of the computed parameters are mostly high. However the accuracy of the skew and the tangential distortion coefficient p_2 calculated in the AgiSoft Lens exceed the computed values and in result cannot be considered as reliable. The positions of the right and the left camera calibrated in the air is shown in figure 37.

Table 5 *Camera calibration parameters of the left and the right camera performed in the air*

Intrinsic parameters	Right camera				Left camera			
	AgiSoft	Accuracy	Toolbox	Accuracy	AgiSoft	Accuracy	Toolbox	Accuracy
fx [mm]	8,314	0,008	8.317	0,006	8,349	0,019	8,347	0,006
fy [mm]	8,313	0,008	8.315	0,006	8,349	0,013	8,347	0,006
cx [mm]	4,492	0,010	4,489	0,007	4,484	0,012	4,488	0,006
cy [mm]	3,396	0,008	3,399	0,006	3,296	0,023	3,392	0,005
Skew [deg]	0,0011	0.0012	0.0003	0.0001	0,0012	0.0013	0.0003	0.0001
k1 [pix^{-2}]	-0.12721	0.00542	-0.12541	0.00374	-0.12213	0.00663	-0.12490	0.00309
k2 [pix^{-4}]	0.19425	0.03369	0.20692	0.02084	0.16676	0.04711	0.20163	0.01704
k3 [pix^{-6}]	-0.07756	0.06167	0.00015	0.00018	-0.00332	0.09953	-0.00012	0.00016
p1 [pix]	0.00044	0.00024	-0.00071	0.00021	-0.00038	0.00026	-0.00023	0.00019

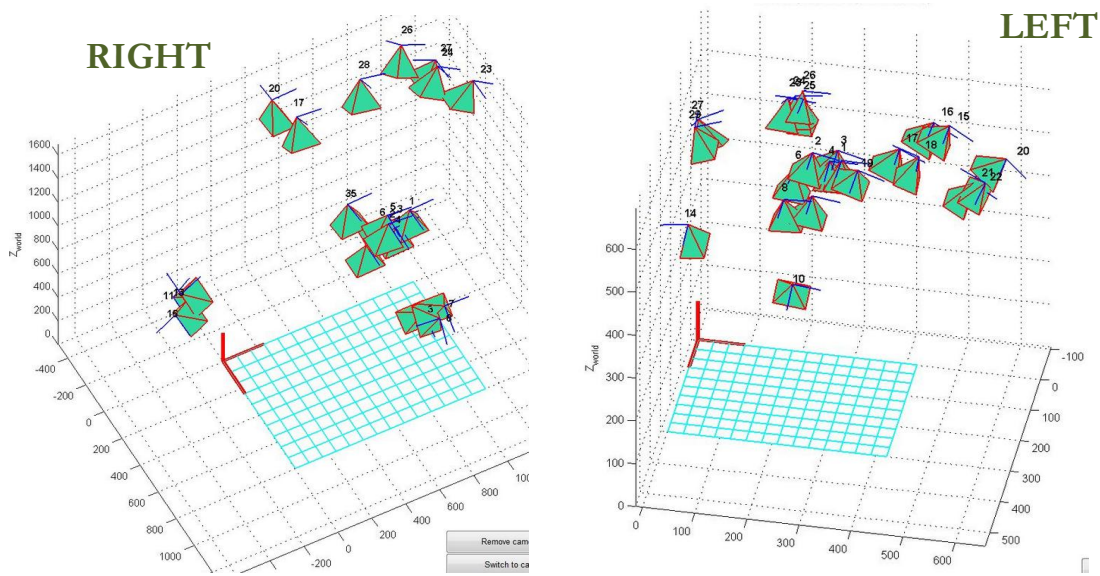| p2 [pix]	-0.00021	0.00031	-0.11059	0.03438	0.00050	0.00031	-0.09583	0.02814

Figure 37 *The positions of the right and the left camera calibrated in the air*

The camera calibration performed in the sea

The calculated preliminary focal length is 11.65 and it is close to the computed focal lengths included in table 6. All computed values by AgiSoft Lens and Camera Calibration Toolbox for MatLab differ significantly from each other. The accuracy of the computed parameters are high.

If we divide the focal lengths of the cameras calibrated in the saltwater and in the air it will turn out that approximate water refractive index is equal around 1.35 and it is close to the assumed value 1.339. The positions of the right and the left camera calibrated in the sea is shown in figure 38.

Table 6 *Camera calibration parameters of the left and the right camera performed in the sea*

Intrinsic parameters	Right camera				Left camera			
	AgiSoft	Accuracy	Toolbox	Accuracy	AgiSoft	Accuracy	Toolbox	Accuracy
fx [mm]	11,216	0,019	11,351	0,079	11,273	0,021	11,208	0,076
fy [mm]	11,105	0,013	11,126	0,056	11,080	0,014	11,088	0,048
cx [mm]	4,233	0,012	4,328	0,086	3,690	0,017	3,859	0,082
cy [mm]	3,453	0,023	3,316	0,116	3,336	0,025	3,585	0,108
Skew [deg]	-0.0696	0.0055	0.0006	0.0030	-0.1667	0.0069	-0.0139	0.0031
k1 [pix^{-2}]	0.11379	0.00952	0.09395	0.04768	0.17510	0.00771	0.11647	0.03100

k2 [pix^{-4}]	0.87851	0.12467	0.67518	0.05026	0.12107	0.07873	0.46175	0.29467
k3 [pix^{-6}]	-0.41499	0.47544	0.01945	0.00333	0.866721	0.23587	0.03045	0.00290
p1 [pix]	0.01729	0.00062	-0.00647	0.00389	0.01957	0.00068	-0.01463	0.00374
p2 [pix]	-0.01088	0.00056	-3.61981	6.31782	-0.02586	0.00075	0.21670	0.99945
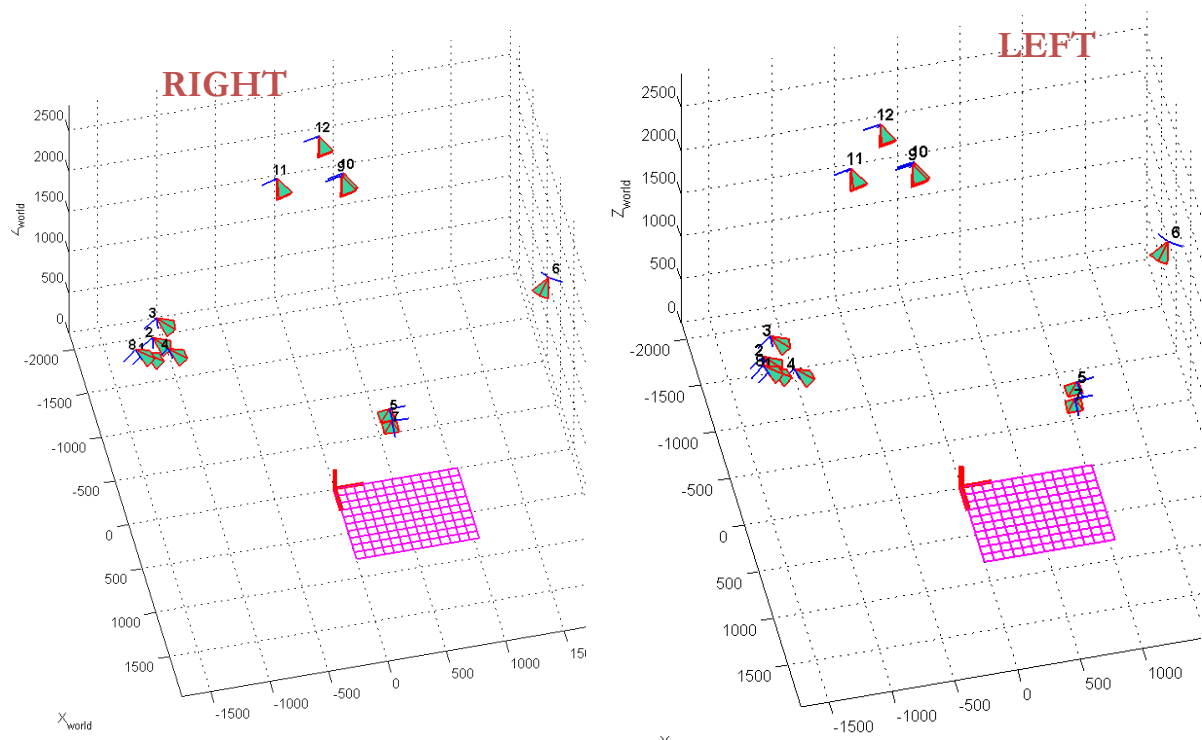
Figure 38 *The positions of the right and the left camera calibrated in the saltwater*

The comparison between these two calibrations results are shown in table 7. The intrinsic parameters of the regular camera and the submerged camera significantly differ from each other. Consequently, the camera calibration process must be performed before each underwater survey.

For the further processes the cameras' intrinsic parameters calculated in Camera Calibration Toolbox for MatLab was chosen. This software computed the final values based on a larger amount of photographs, especially including the rotated images. In consequence, the intrinsic parameters of the cameras calculated in that software is assumed to be more reliable than in AgiSoft Lens.

Table 7 *Comparison of the intrinsic parameters computed in the both software.*

Intrinsic	Calibration in the air		Calibration in the sea	

parameters	Right camera		Left camera		Right camera		Left camera	
	AgiSoft	Toolbox	AgiSoft	Toolbox	AgiSoft	Toolbox	AgiSoft	Toolbox
fx [mm]	8,314	8.317	8,349	8,347	11,216	11,351	11,273	11,208
fy [mm]	8,313	8,315	8,349	8,347	11,105	11,126	11,080	11,088
cx [mm]	4,492	4,489	4,284	4,488	4,233	4,328	3,690	3,859
cy [mm]	3,396	3,399	3,296	3,392	3,453	3,316	3,336	3,585
Skew [deg]	0,0011	0.0003	0,0012	0.0003	-0,0696	0.0006	-0,1667	-0.0139
k1 [pix^{-2}]	-0.12721	-0.12541	-0.12213	-0.12490	0.11379	0.09395	0.17510	0.11647
k2 [pix^{-4}]	0.19425	0.20692	0.16676	0.20163	0.87851	1.67518	0.12107	0.46175
k3 [pix^{-6}]	-0.07756	0.00015	-0.00632	-0.00012	-0.41499	0.01945	0.86672	0.03045
p1 [pix]	0.00044	-0.00071	-0.00038	-0.00023	0.01729	-0.00647	0.01957	-0.01463
p2 [pix]	-0.00020	-0.11059	0.00050	-0.09583	-0.01088	-3.61981	-0.02586	0.21670

The extrinsic parameters of the stereo pairs calculated by Camera Calibration Toolbox for MatLab in the air and in the saltwater are given in table 8. The air stereo pair calibration is very accurate. The calculated distance between the cameras is 31,001 cm and it is equal to the distance measured manually by a ruler during the measurement (31 cm). As it is clearly seen on figure 39 the positions of the cameras are accurately placed in the same line.

Table 8 *Extrinsic parameters (position of the right camera with respect to the left camera)*

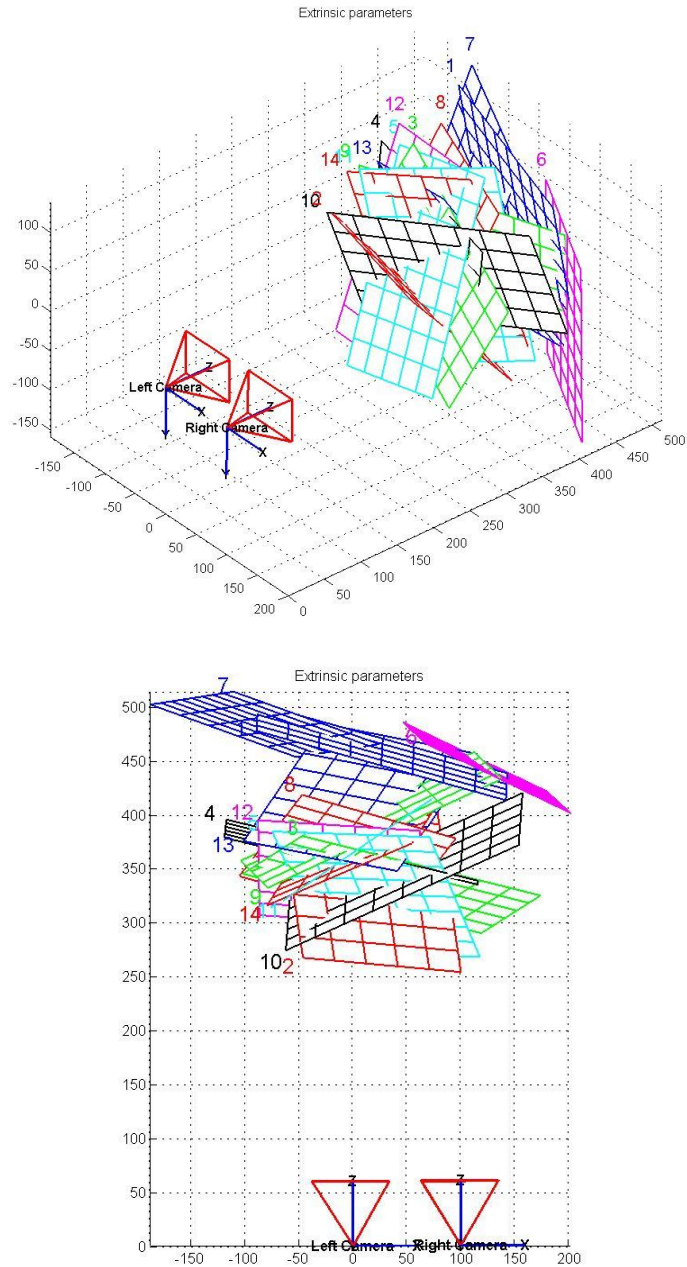|	Translation vector			Rotation vector			The measured distance between two cameras [cm]	The calculated distance between two cameras [cm]
	X [mm]	Y [mm]	Z [mm]	φ [deg]	ω [deg]	ϰ [deg]		
Air	-310.080	0.312	2.346	-0.00298	0.04123	0.00148	31	31,001
Saltwater	-426.560	-20.641	48.909	-0.01416	-0.04151	0.04770	42	42,985

Figure 39 *The camera and the calibration sheet positions of the stero pair*

The extrinsic parameters calculated for the submerged stereo pair are not reliable due to the fact that the photographs were not taken simultaneously. The vehicle was moving with 0.2 m/s speed and the time difference between the exposures was around 0.1 second. In result the vehicle changed its position by approximately 2 cm between these two exposures. This variation is very easy to notice in the plot from Camera Calibration Toolbox for MatLab (figure 40). The position of the left camera is shifted with respect to the right one. The calculated Z value of the translate vector indicates that the vehicle could move around 5 cm between the two exposures of the right and the left camera. In addition a distance between these two cameras are 42,985 cm (table 8). The difference between the computed value and the manually measured distance is not that large and it is equal 1 cm.
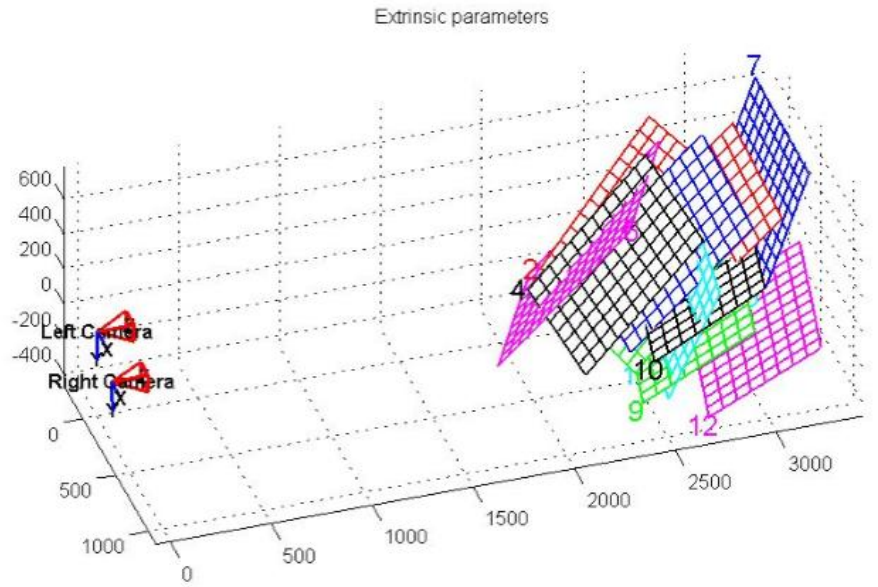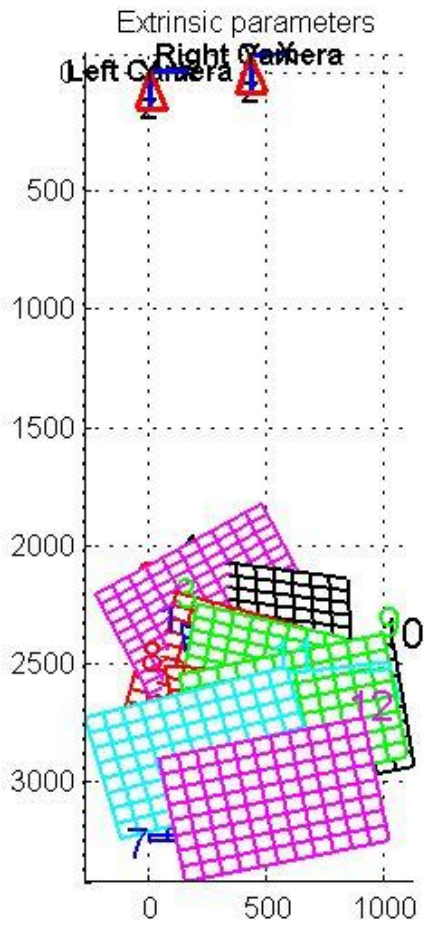
Figure 40 *The camera and the calibration sheet positions of the submerged stero pair*

5.3 3D model generation

The underwater object

177 colour corrected photographs were loaded to AgiSoft PhotoScan. Photographs taken from the left and the right camera were sorted and calibrated accordingly to the left and right camera calibration files. The camera positions and their orientation were computed by the "Align photos" command. Photographs were aligned with a high accuracy and a generic pair selection which allowed to decrease time of the process by preselecting the overlapping pair of photos before the main align process. In result a sparse point cloud model were produced. The sparse cloud and the calculated cameras' positions are shown in the figure 41. The photographs evenly cover the entire underwater object from the all sides.
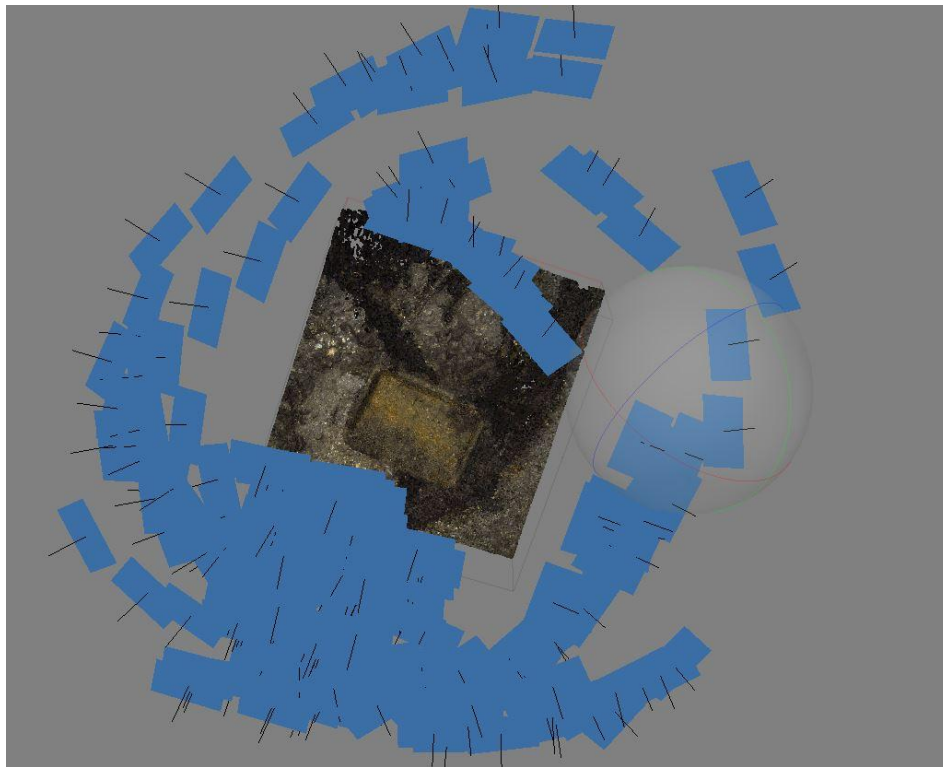
Figure 41 *The sparse cloud and the cameras' positions generated by PhotoScan*

The valid part of the object was selected and a few high quality dense point clouds were produced using various depth filtering options: *Aggressive*, *Moderate* and *Mild*. The Mild depth filtering selection provides the highest feature reconstruction level and it should be used when improved accuracy is required. The *Aggressive* mode corrects the dense cloud and deletes the protruding points from the model. In result less detailed point cloud is created. The *Moderate* option gives result between the *Aggressive* and *Mild* depth filtering options (Photoscan, 2013). The comparison of these three depth filtering methods of the point cloud is shown in figures 42 and 43.

Figure 42 *Comparison of Aggressive, Moderate and Mild depth filtering modes – top view*
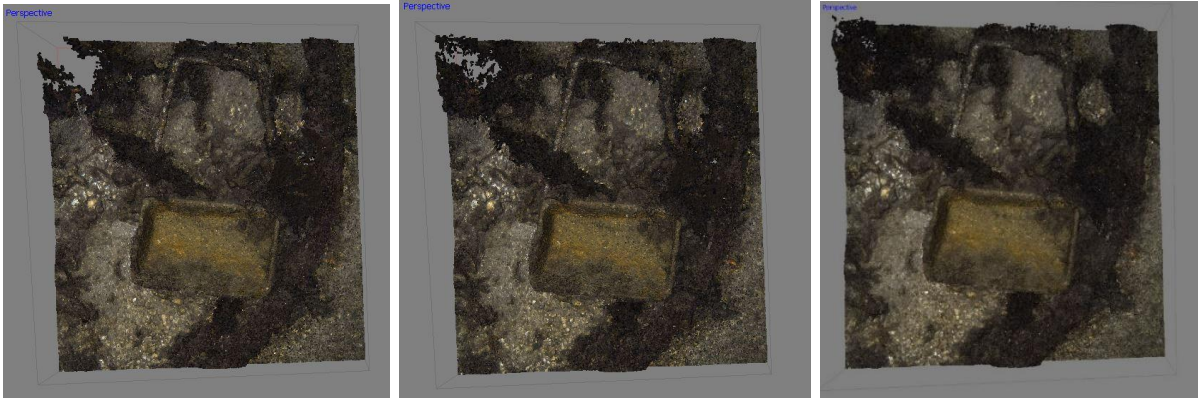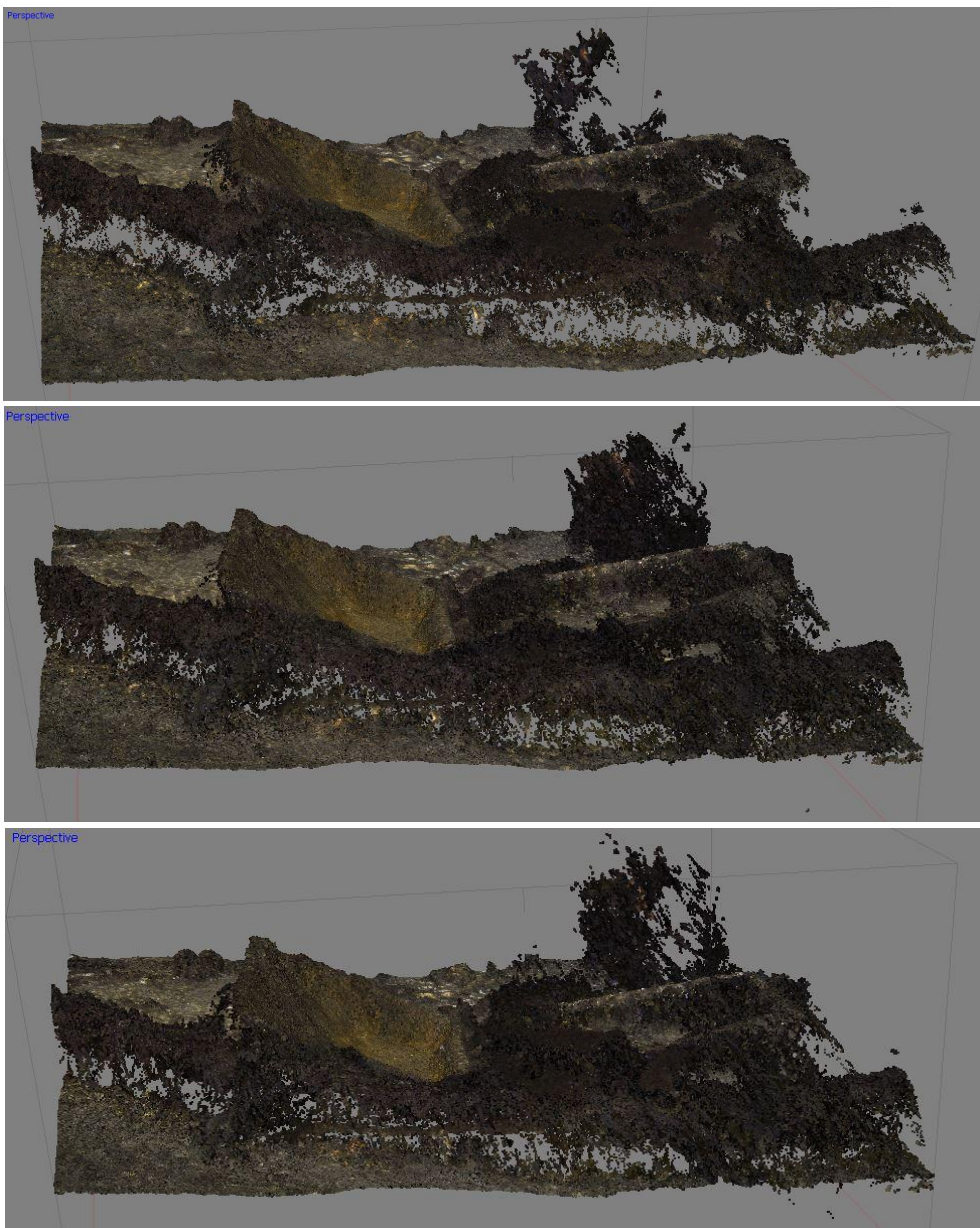

Figure 43 *Comparison of Aggressive, Moderate and Mild depth filtering modes – side view*

The *Aggressive* depth filtering mode created an insufficient numbers of points. The resulted dense cloud has a lot of holes, in particular in places where seaweed or poor image coverage occurred. This mode properly removes unnecessary points. However, in result an incomplete model was created. The *Aggressive* depth filtered dense cloud was too low quality and will not be used in further processing. The *Moderate* depth filtering mode reconstructed the underwater model well. The seaweed is fairly well preserved comparing to the other filtering options. The *Mild* depth filtering mode provided more disordered result however it preserved more points in comparison to the other methods. Moreover, this mode reconstructed the largest amount of individual features.

Before further processing, the inaccurate or supplementary points of the dense cloud should be manually removed. Nevertheless this process in PhotoModeler software is very imprecise and it easily eliminates both unnecessary and required points during this procedure so it will not be used in this project.

The mesh will be created both in PhotoScan and Geomagic. In PhotoScan the process will be conducted using only "*Mild*" dense cloud. Further processes will be conducted in Geomagic using the *Moderate* and the *Mild* depth filtered dense cloud. The "*Mild*" and the "*Moderate*" dense point clouds were exported to the PLY (Polygon File Format) format that contains points' coordinates and additional information about their colour.

3D polygonal object created in the AgiSoft PhotoScan.

The underwater object was reconstructed using *Built Mesh* command. Number of polygons in the final mesh were set to 1500000 and the surface type was assigned to arbitrary which was recommended by the software for this structure. Three 3D polygon objects were created automatically using three different methods: without interpolation, with interpolation and with extrapolation of the dense point cloud.

In the first case no interpolation technique was used. Due to fact that the only surrounding points of the dense cloud were connected in triangles the final object has a lot of holes (figure 44). The seabed are reconstructed very well however in the places where seaweed or poor coverage occurred the model is incomplete. The shovel is fairly well reconstructed taking into account the fact that the bottom – left corner of the object does not stand out from the background.
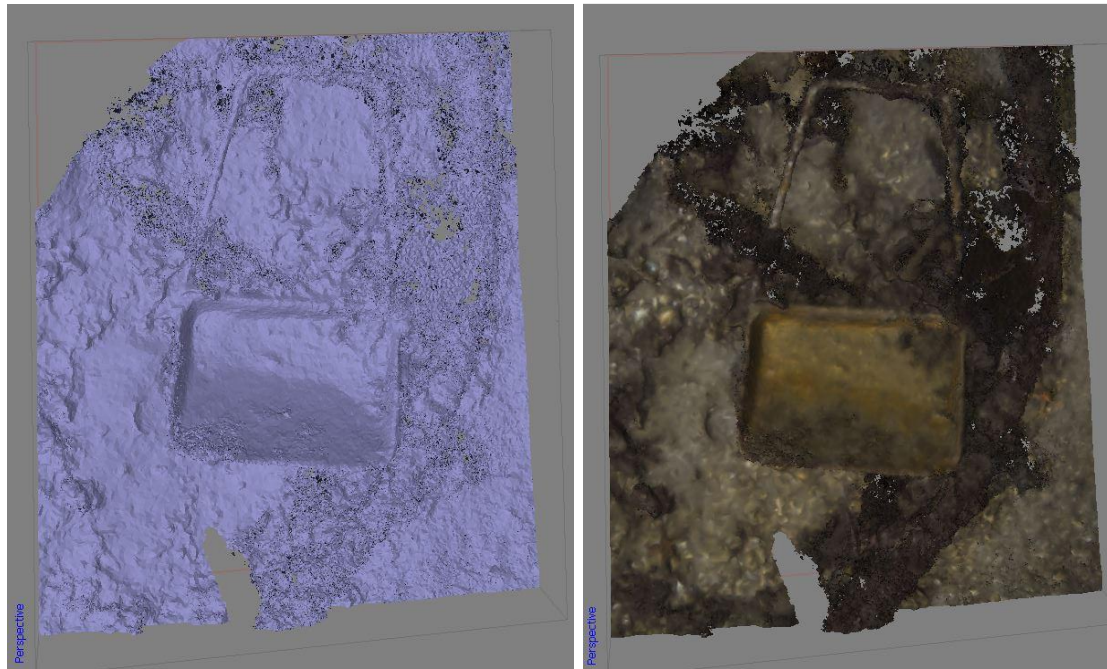
Figure 44 *3D polygon object constructed without interpolation technique presented in shaded and solid mode*

In order to enhance the object's structure *Close Holes* feature was used to fill up existing holes. The algorithm used in PhotoModeler is very basic and it does not allow to choose any particular filling preferences. The default setting fills up holes with a flat surface which in most cases do not reflect the actual characteristic of the object. The only parameter that can be set in this command is the size of holes which will be filled. However the analysed object cannot be reconstructed properly using this option. A high value of this feature ruins the geometry of the object which in consequence leads to a poor result. On the contrary a low value does not influence the 3D polygon object much (figure 45).
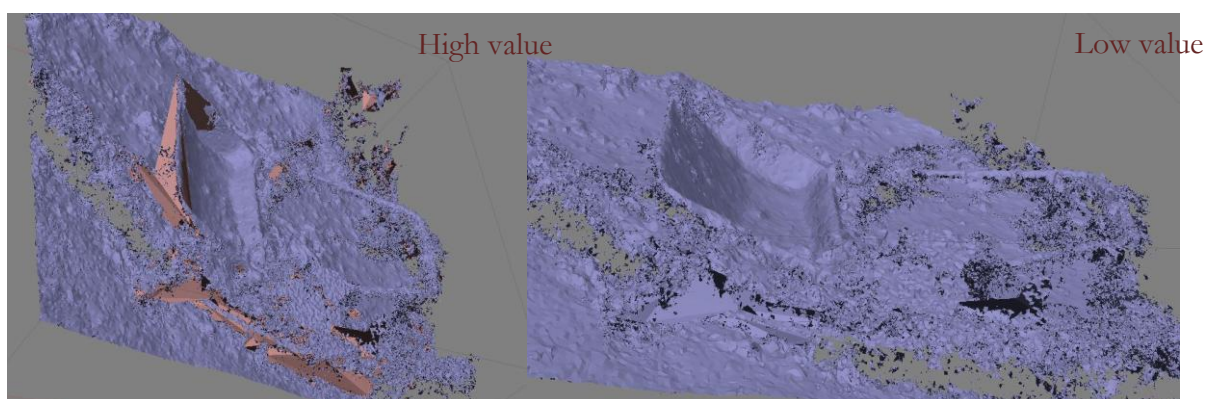

Figure 45 *Different values of "Fill Holes" command of the 3D polygon object constructed without interpolation technique*

Respectively the extrapolated 3D object reconstruction mode were used. This technique provides a smooth model without any holes. The new, additional points are estimated outside the known range based on its relationship with the existing dense cloud points

(Photoscan, 2013). The advantage of this technique is solid model. However this technique tends to produce incorrect additional polygons. Seaweed and poor coverage places are well reconstructed but the bottom – left corner of the shovel is missing data. No additional operations were conducted on this mesh due to fact that this algorithm filled up all holes. The 3D polygon object constructed using this technique is shown in the figure 46.
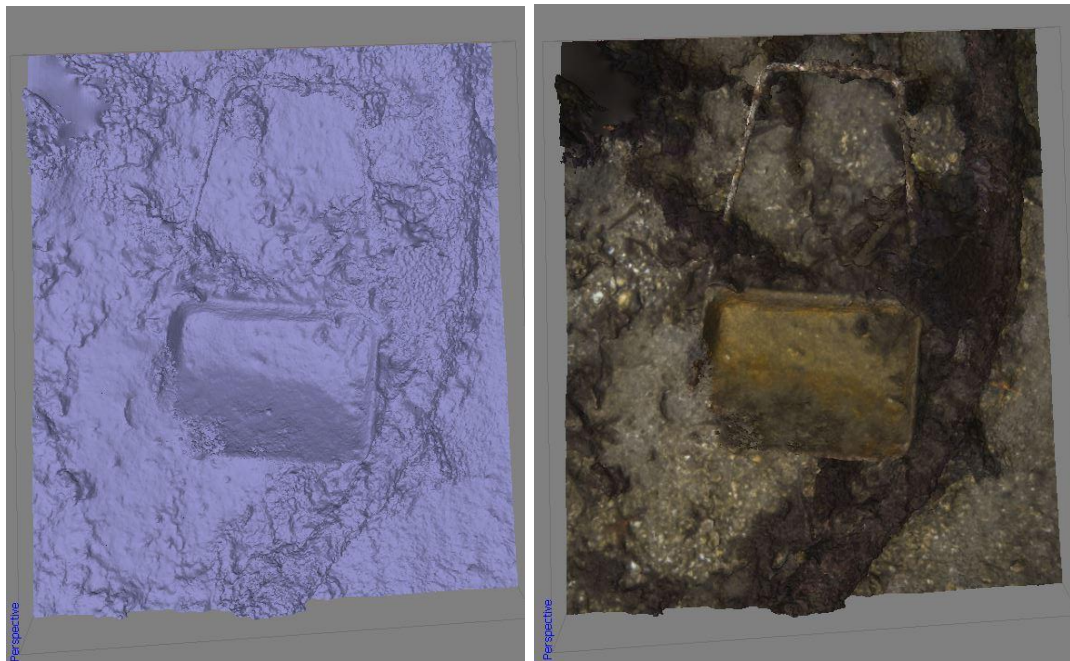
Figure 46 *3D polygon object constructed with extrapolation technique presented in shaded and solid mode*

The last technique used is an object reconstruction based on the interpolation method. This setting allows us to construct solid surface by inserting additional points between already existed dense cloud points within a range of a particular radius. Predominantly the underwater object was properly reconstructed. However the bottom – left corner of the shovel is still incomplete. In comparison to the previous methods, the interpolation technique provides the most detailed result. The created seabed does not differ from the one which is produced using the extrapolated technique. However the seaweed and the shovel is better constructed using the interpolated technique. No additional operations such as filling holes were performed on this model. The 3D polygon object constructed using this technique is shown in the figure 47.
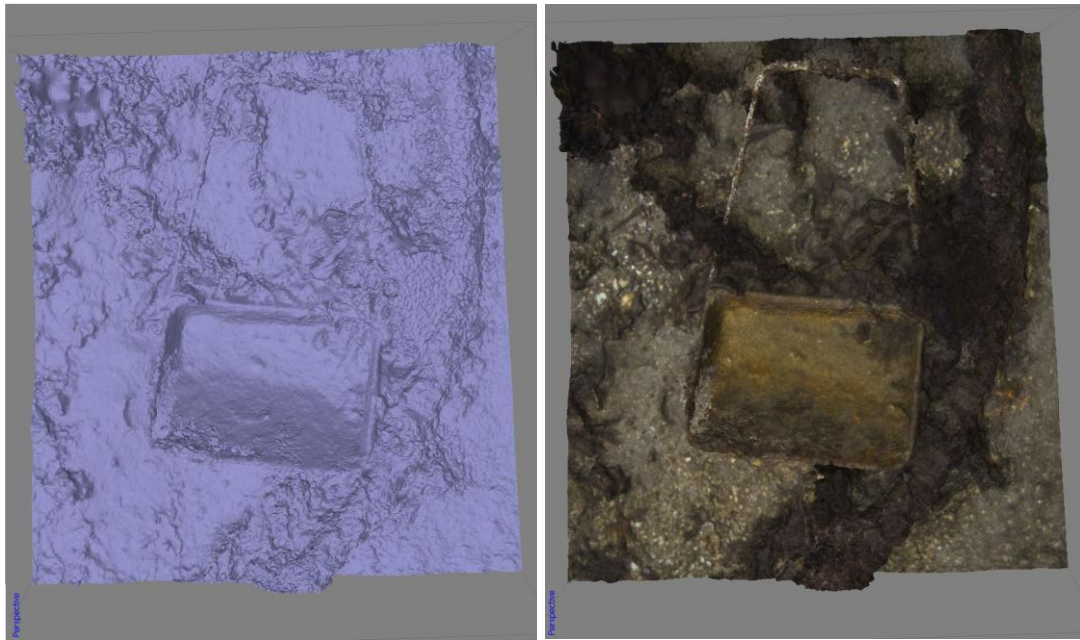
Figure 47 *3D polygon object constructed with interpolation technique presented in shaded and solid mode*

Three close-ups of the 3D model (the shovel, the handle and the poor photo covered part of the object) were generated and compared. The first model, created without any interpolation technique reconstructed the shovel the most accurately. The dense cloud in the one corner of the shovel is not very consistent. This is due to a small difference in colour between the seabed and the shovel. The part of the shovel coalesced with the background. However regardless of the poor data, the first technique managed to reconstruct the shovel quite accurately. Algorithms used by the software in interpolated and extrapolated methods have not been able to reconstruct this area well and it removed a lot of data (figure 48).

Without interpolation   **Interpolated**   **Extrapolated**

Figure 48 *Model of the shovel created by three different techniques*

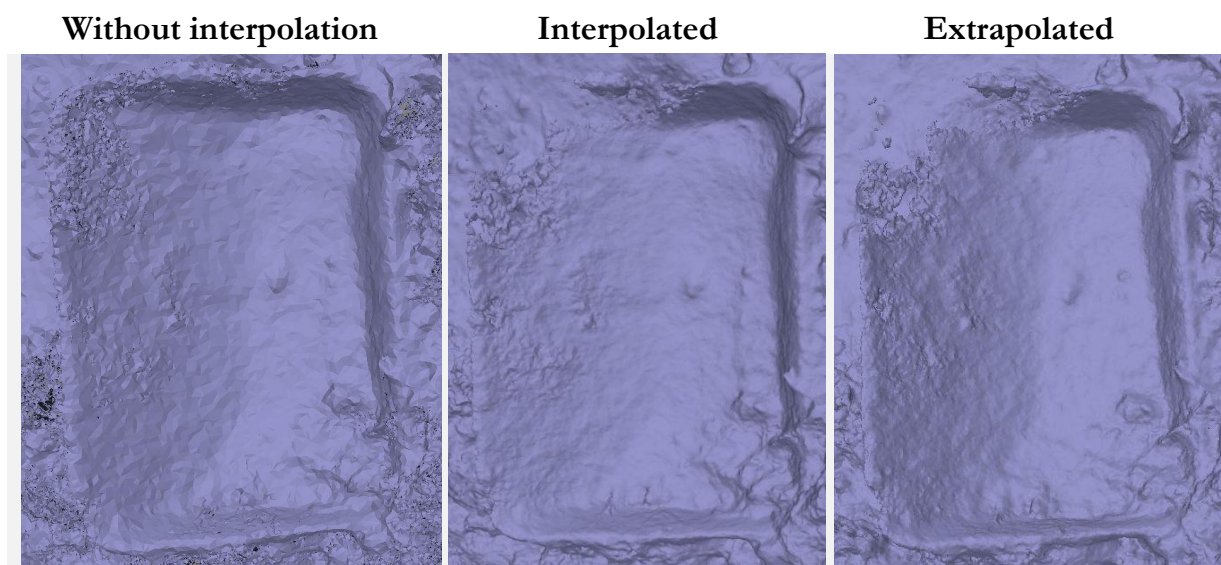The handle of the shovel was not reconstructed well in any of the presented techniques (figure 49). It is caused by the moving seaweed which entwined the handle and in result influenced the geometry and aspect of the dense cloud. The model created without any interpolation technique reconstructed the handle the closest to its true appearance. However a lot of disconnected polygons appeared around the handle. The other techniques managed to connect points into polygons but in result the handle become very distorted.
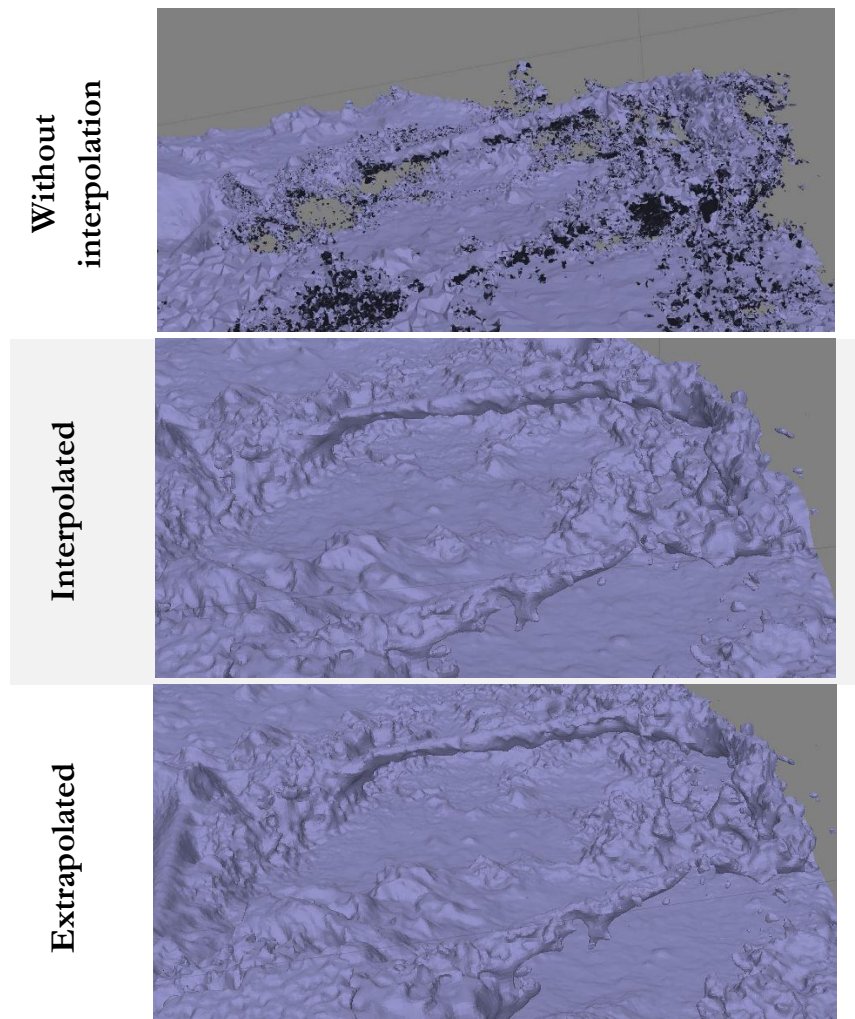
Figure 49 *Model of the handle created by three different techniques*

The part of the object with a poor photo coverage created without using any interpolation techniques did not fill up any holes (figure 50). The mesh is rough and irregular and a lot of disconnected polygons occurred. On the other hand interpolation and extrapolation method worked very well in this situation. In addition objects created by interpolated and extrapolated method do not differ much from each other.

Figure 50 *Model of a poor photo covered part of the object created by three different techniques*

The last step of the 3D modelling is a building a model texture. PhotoScan allow us to use a few texture mapping modes: *Generic*, *Adaptive ortophoto*, *Ortophoto*, *Spherical*, *Single Photo* and *Keep uv*. The choice of the texturing mode should be dependent on the structure of the object. The *Ortophoto and Adaptive ortophoto* modes should be used for flat areas due to fact that both algorithms project the textures using orthographic projection. *Spherical* mapping mode should be used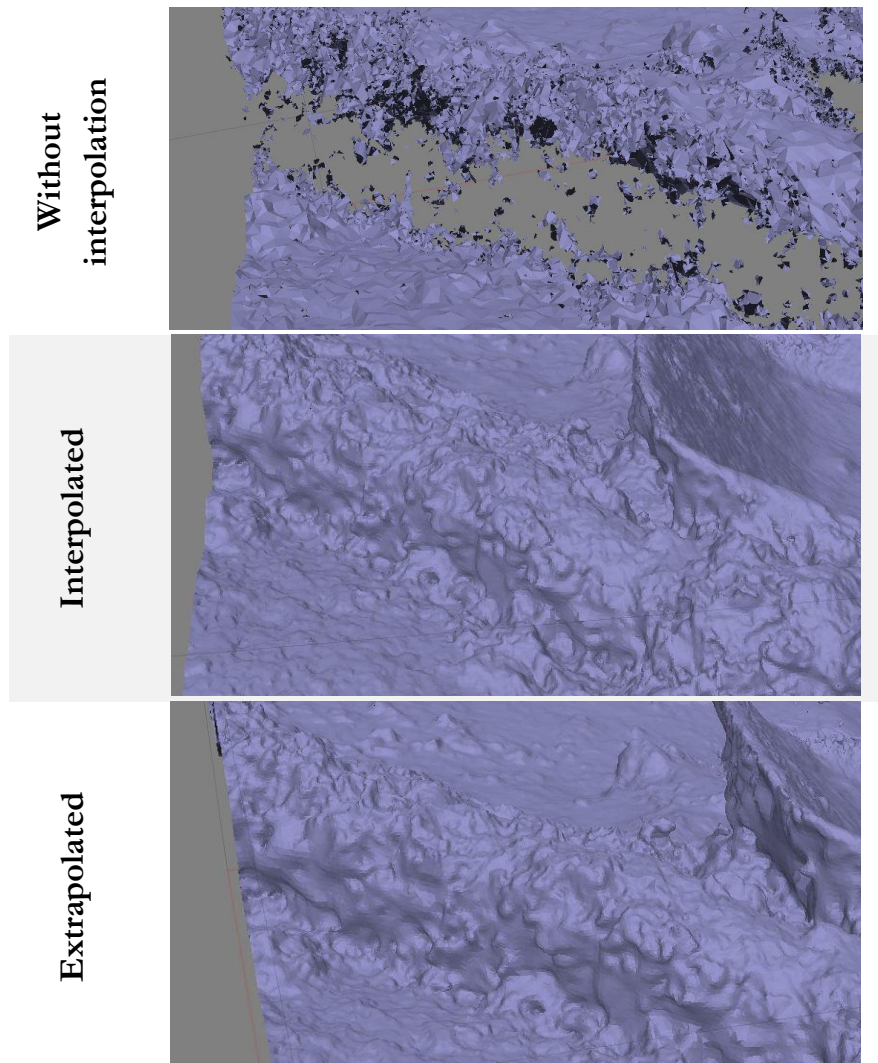 only for ball-shaped forms. Aim of the *Single photo* mode is formation of texture based on only one chosen photograph. Default, generic mode can be used for any kind of shapes. This algorithm does not work based on any preliminary type of the surface, thus it works very well with the non-uniform shape of the object. *Keep uv* command allows us to reconstruct texture using different parameters (for example higher resolution) (Photoscan, 2013). Two texture mapping techniques were used: *Generic* using average and maximum intensity of all pixel values and *Adaptive ortophoto* using maximum intensity value of the all pixels. Additionally colour correction mode was chosen due to high brightness and colour variations between the underwater photographs.

The best texture was created using the *Generic* technique computed with the average value of the all pixels. Texture corresponds to the real appearance of the shovel. Final colours are quite haze however the individual details are still well recognizable. The texture created based on the maximum intensity value of the all pixels are very bright and blurry. Single features are poorly recognizable. *Adaptive ortophoto* mode did not produce a correct texture due to an orthographic projection used in this method. The handle has been reprojected additionally on the seabed, resulting in the confusing result. Dense cloud, coloured mesh created based on the dense cloud colours and three resulting models are shown in figure 51. Textures were built for a polygonal model which was created using the interpolation technique.

Coloured mesh created based on the dense cloud colours

Generic
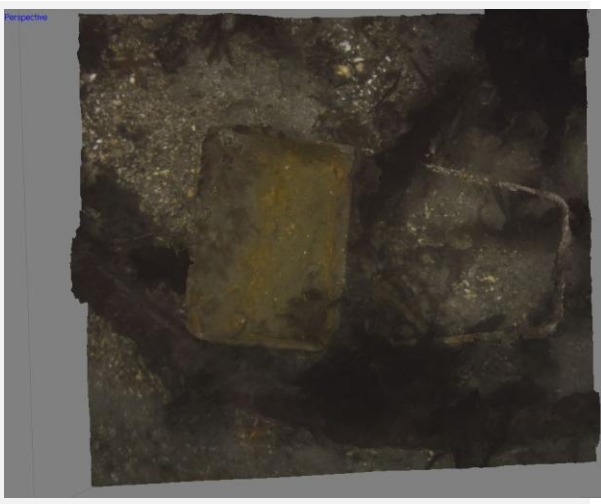
Generic with maximum intensity

Adaptive ortophoto
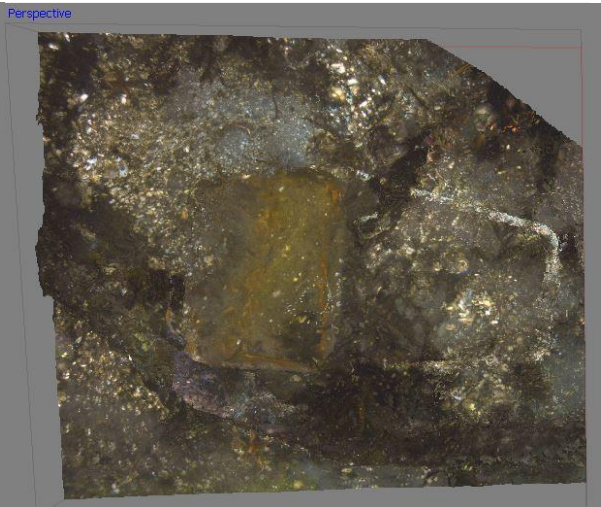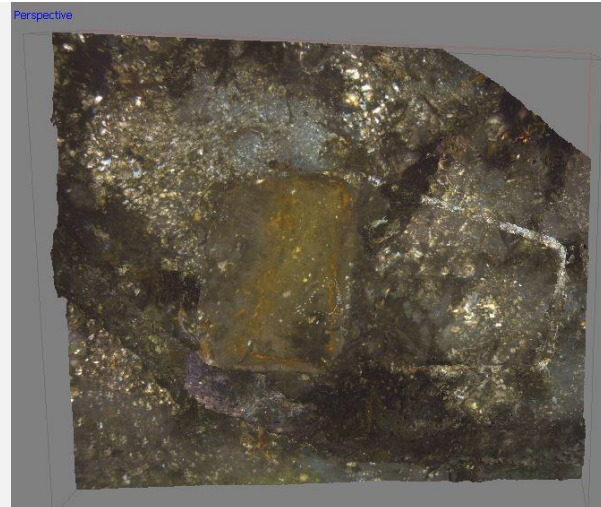
Figure 51 *Different texturizing techniques available in the AgiSoft PhotoScan*

The model created based on the interpolation technique with generic texture using average value of the all pixels is exported to the *3D pdf* file which is available electronically with this thesis in appendix 1.

3D polygonal object created in Geomagic.

The *Moderate* dense cloud were imported to Geomagic and filtered. Variable positions of the seaweed on the subsequent photographs resulted in an inaccurate and incomplete model. The biggest point disorder were seen quite well on the object's handle which was fully covered by the hanging seaweed (figure 52).

Figure 52 *Seaweed covering up the actual surface of the object*

The points which were considered as seaweed entangling the underwater object were removed in order to clean the model and reveal the true characteristic of the object. Additional points were removed carefully so the geometry of the underwater object would not change significantly (figure 53).

Figure 53 *Removal of the seaweed from the underwater model*

Afterwards the dense cloud were filtered automatically using a few functions in Geomagic. Firstly the disconnected components were selected and deleted using the *Disconnected Points* option with separation value set to low. Next, the points were ordered using the *Reduce Noise* command using prismatic shapes (aggressive) mode and medium smoothness level. These options allows us to preserve the real characteristics of the object by maintaining the sharpness of the features. Due to fact that this function does not remove noise on the object's edges, it fits points properly to the various planes such as a plane or sphere (Geomagic Studio 2014, 2014).

After all adjustments a polygon object was created using surface wrapping. The model was created using the maximum degree of the noise reduction and additional removal of the small components. Moreover *Optimize for Spare Data* option was used to help to wrap very unordered points and fill more holes. Additionally every hole below 15 unit will be filled automatically during the process. Maximum number of the resulting triangles were set to 1500000.

All previously described operations were conducted both on the "*Mild*" and "*Moderate*" dense point clouds and compared (figure 54). The polygon object created from the "*Moderate*" dense point cloud are less accurate and more incomplete in comparison to the polygon object created from "*Mild*" data set. A large number of big holes occurred on the "*Moderate*" dense point cloud especially in the places where seaweed occurred. This model provides better filtered result where single objects are more recognizable. However a lot of data is lost. The "*Mild*" polygon object has more noise but the surface is better reconstructed comparing to the other model. The green structures on both models indicate mesh errors.
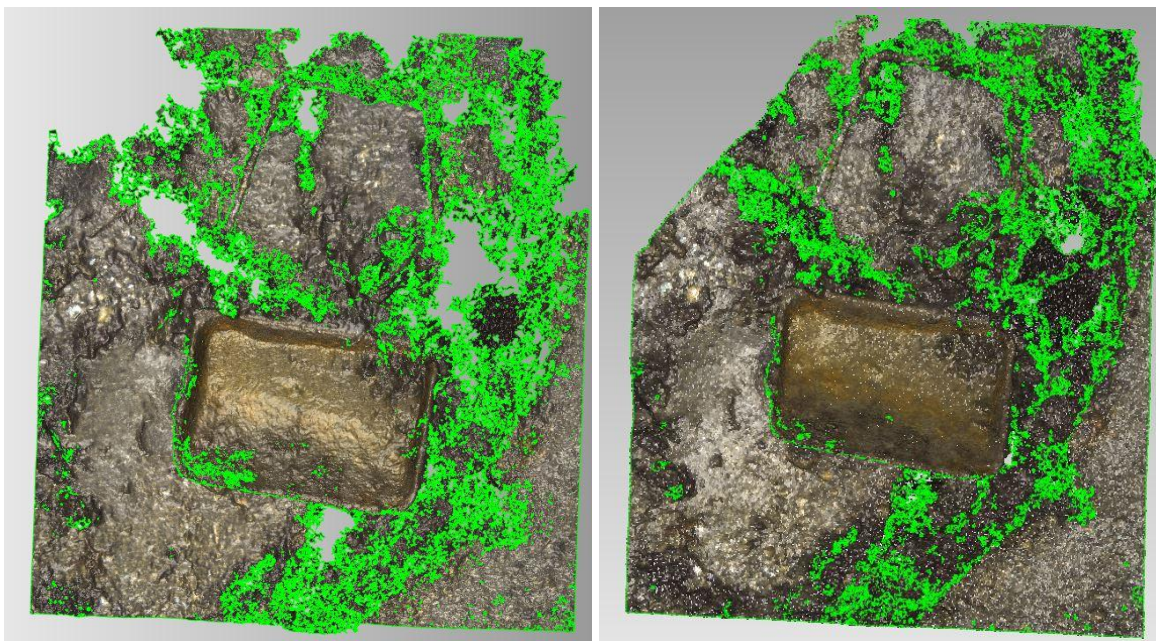
Further processes will be conducted in Geomagic using the polygon model constructed from the *Mild* depth filtered dense cloud.

The polygon object were automatically repaired using the Mesh Doctor tool. The process were conducted using the default settings of this command. The following problems were repaired during this process:

- Non-Manifold Edges (triangles present on the edge of the mesh that are connected to the mesh just on the one side).
- Self-Intersections (triangles which are twisted or twined together with situated next to or very close to the other triangles).
- Highly-Creased Edges (triangles that are next to and joined with each other at sharp angles).
- Spikes (sets of minimum three triangles which are visible as a point on a mostly-smooth polygon object).
- Small Components (sets of disconnected triangles which are protruding from the mesh).
- Small Tunnels (double-layered formations in the polygonal objecct with a front and back opening)
- Small Holes (small hollow spaces in the 3D polygon mesh).

Description of the above errors is obtained from the Geomagic Studio 2014 Manual (Geomagic Studio 2014, 2014).

The remaining holes were filled both automatically and manually using the *Fill Holes* command. There are three filling options: *curvature*, *tangent* and *flat*. The *Curvature* and the *tangent* techniques both compute new polygons based on the curvature of the surrounding mesh but the *tangent* option does not significantly change the geometry of the object like the *curvature* one. The flat technique fills up holes with a basic flat surface (Photoscan, 2013). The graphical representation of these 3 techniques are shown in figure 55.
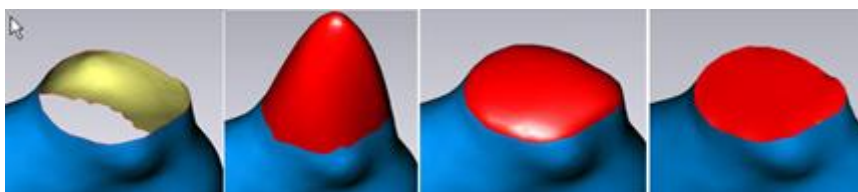
Figure 55 *Different filling holes techniques: curvature, tangent and flat (Geomagic Studio 2014, 2014)*

Smaller holes were filled in automatically using the *tangent* filling hole technique. The remaining big holes were filled manually using the curvature, tangent or flat technique depending on the existing holes and their surroundings. Example of the structures filled up by the *Fill holes* command using tangent and flat option is shown in figure 56.

Figure 56 *Holes filled by the tangent (1) and the flat (2) technique*

The final result after all necessary adjustments is shown in figure 57. Geomagic managed to produce the polygonal model of the shovel quite precisely. Both the seabed and the shovel are reconstructed very well. Nevertheless the result do not look very natural in the parts of the object where the big holes were manually filled out. The shape of the handle and the seaweed are of poor quality and extremely noisy.
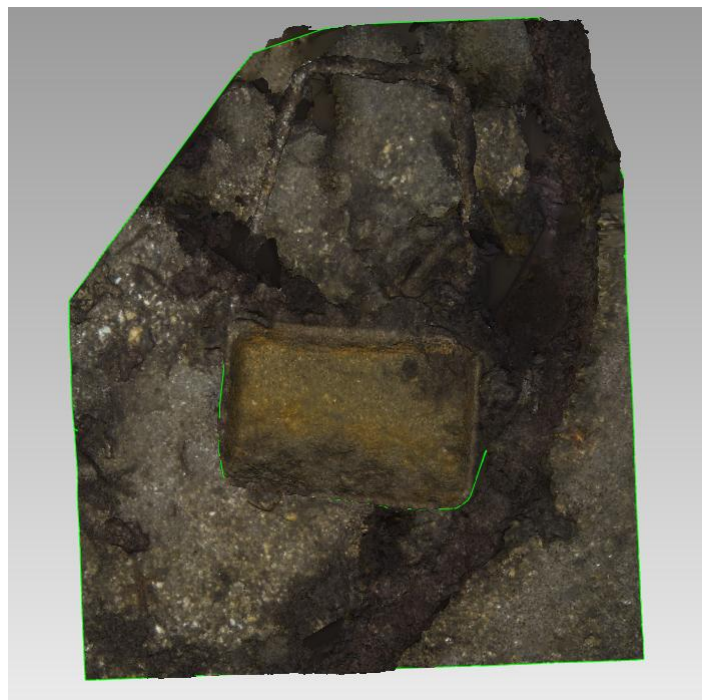
Figure 57 *The polygonal model of the underwater object*

A few close-ups of the shovel, the handle and a poor photo covered part of the polygon object were made. The shovel are reconstructed very well on this model. The shovel are solid and without any holes. In comparison to the previous software, Geomagic allowed us to leave the empty space under the shovel without the need to combine the surrounding triangles. In consequence the model presents the actual shovel's surface (figure 58).
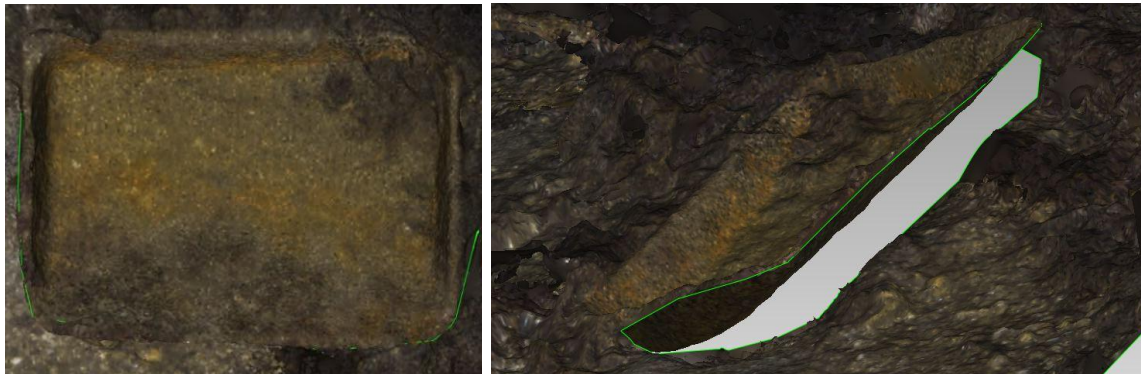
Figure 58 *Close-up of the shovel generated by Geomagic*

The handles original shape were very well preserved. The upper side of the handle is better reconstructed then the bottom side which was covered by the hanging seaweed. Despite the fact that mesh correction was performed a lot of non-manifold edges occurred on the handle (figure 59).

Figure 59 *Close-up of the handle generated by Geomagic*

The poor photo covered part of the object were entirely filled up manually using the tangent filling holes technique. The created mesh is smooth and looks very artificial (**figure**). Additionally this process tends to merge disconnected triangles with the mesh and produce poor result that affects the final geometry (dark brown structures).
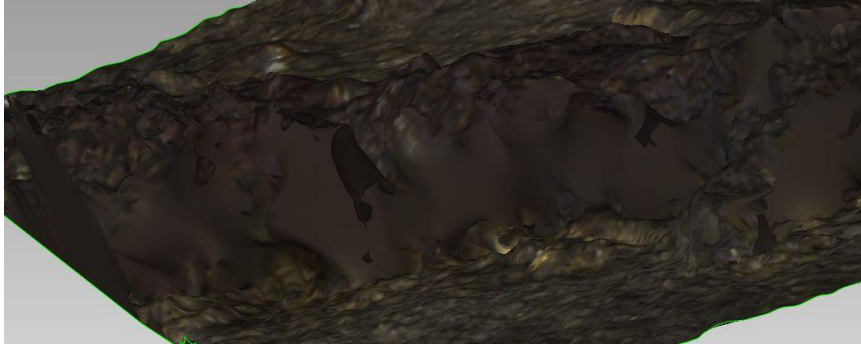
Figure 60 *Close-up of a poor photo covered part of the object*

Finally a model texture was created. The photographs have been projected on the polygon object manually by selecting corresponding points between the photograph and the model. The procedure has been continued until the model position corresponds to the position of the object on the photograph. Additional feature *blend* combined new image colour with an existing texture colour. However this option did not work well on this project (figure 60). The colours of the photographs used in this project differed too much from each other and the process failed. The texturizing result is not satisfactory therefore texture generated from the point cloud colours will be used.
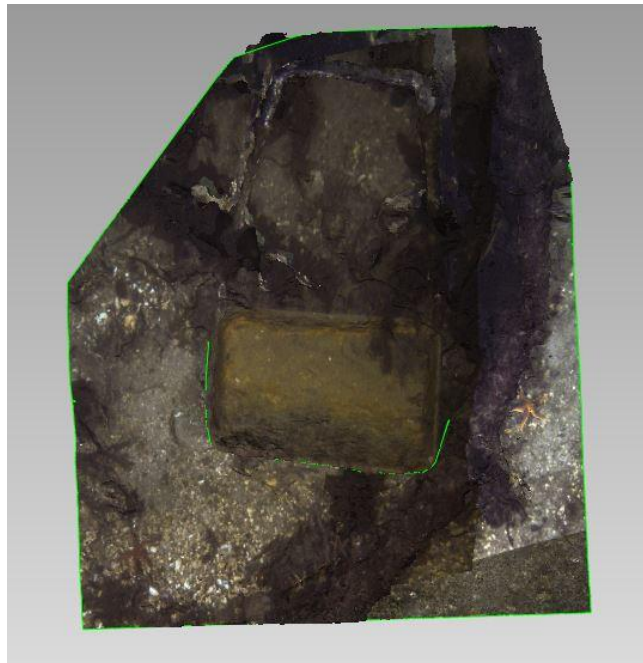
Figure 61 *Textures generated in the Geomagic software*

The model created in Geomagic is exported to the *3D pdf* file which is available electronically with this thesis in appendix 2.

The *Mild* depth filtered dense cloud were created in PhotoScan accordingly to the previously presented methods. The sparse cloud and the calculated cameras' positions are shown in figure 62.
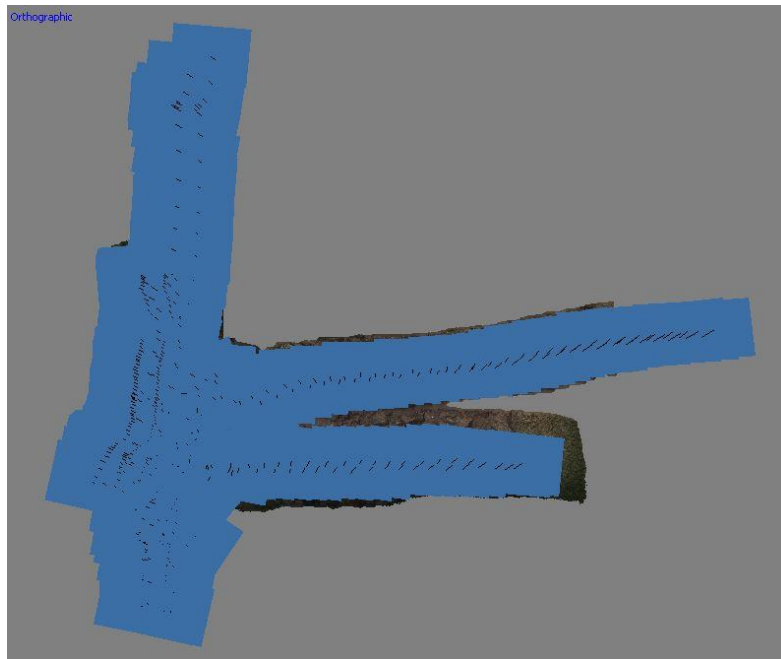
Figure 62 *The sparse cloud and the cameras' positions generated by PhotoScan*

The dense cloud and the cameras positions are distorted due to lack of external data (no scale bar, ground control points on the scene and no preliminary positions of the cameras) and no common coverage between two strips. As it is shown in figure 63 camera positions are curving down to the seabed.
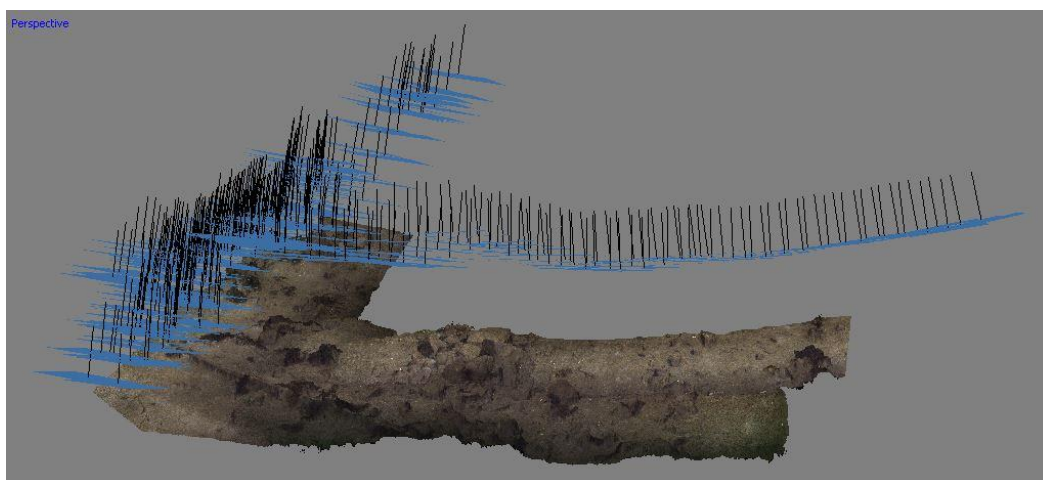
Figure 63 *Deviations of the camera's positions*

The underwater pipeline was reconstructed using the *Built Mesh* command. The maximum number of polygons in the mesh were set to 8500000 and the surface type was assigned to arbitrary which was recommended by the software for this structure. The 3D polygon objects were created automatically based on the interpolation technique. The created mesh shows in detail deviations of the model's shape (figure 64). The object is curving down in the middle. The biggest difference can be seen on these two disconnected strips. The strips are pointing out into two different directions. Moreover the shorter strip steer more upwards then the longer one thereby resulting in incorrect model.
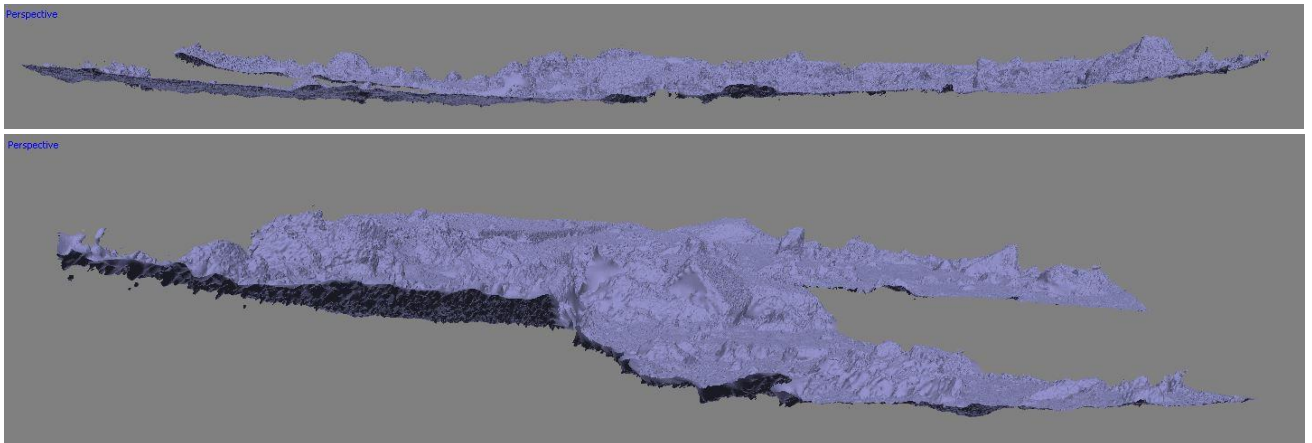

Figure 64 *Deviation of the shape of the created model*

Afterwards the texture was created using the *Generic* technique computed with the average value of the all pixels. The texture corresponds to the real appearance of both the seabed and the pipeline. The shaded mesh and the textured mesh are shown in figure 65**.** The texture brightness is not consistent along the whole object. Places where edges of the photographs are seen are darker. Due to fact that light is highly absorbed under water the centre of photographs are better illuminated then the edge.
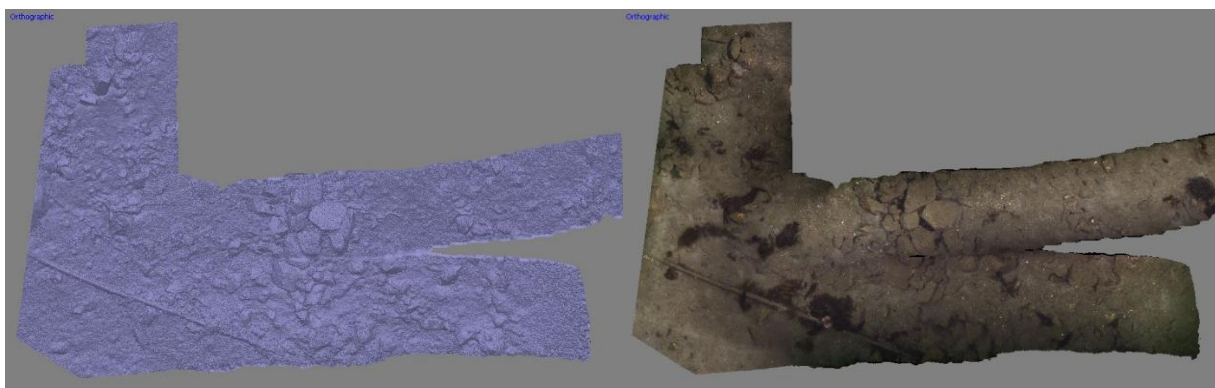
Figure 65 *The shaded model and the textured model of the underwater pipeline*

The seaweed has a negative impact on the result. The seaweed which is winded around the pipeline deforms the model. The structure created in places where seaweed occurred does not resemble the actual object and in result it cannot be accepted. Despite the previous fact the final mesh is very accurate. Even very small objects such as a thin cable seen in figure 66 are well reconstructed. Additionally the appearance of the other parts of the mesh such as seabed or rocks highly corresponds to the actual structure.
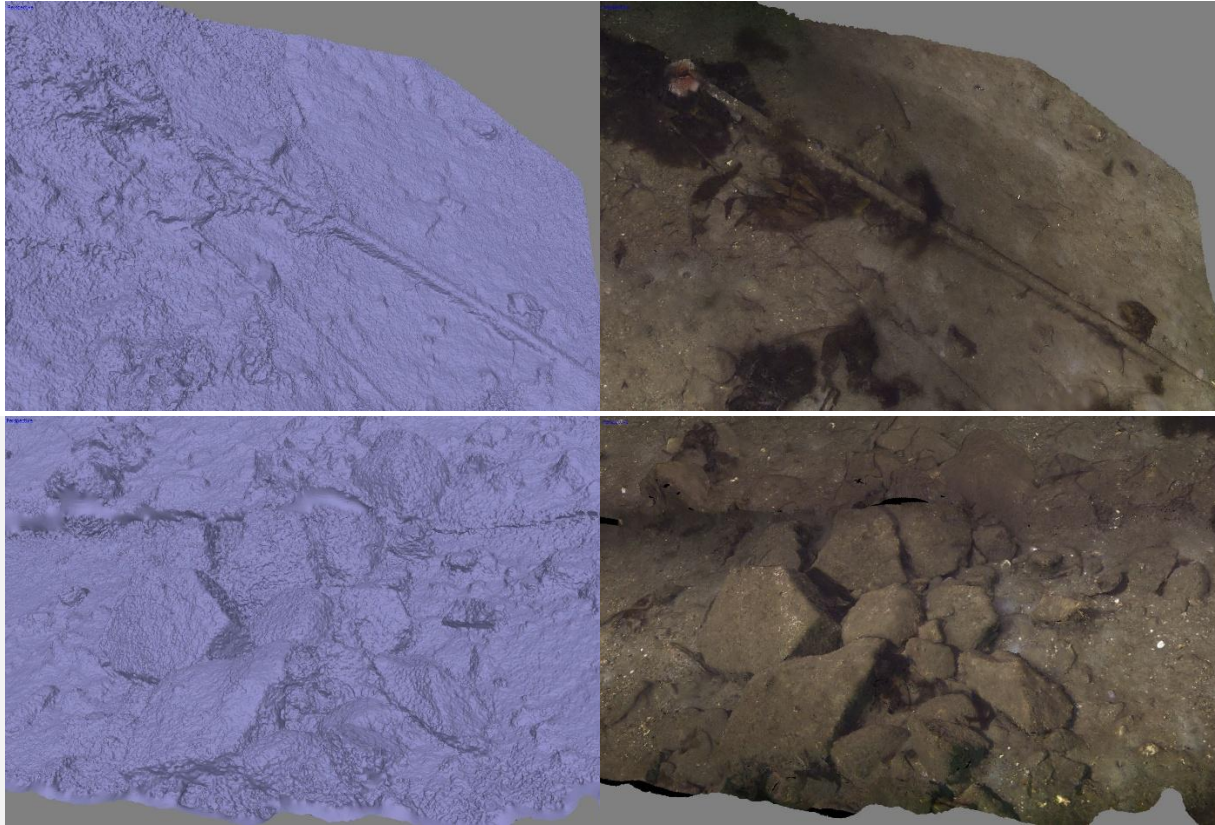
Figure 66 The close-ups of the underwater pipeline and rocks

The model of the pipeline created based on the interpolation technique with generic texture using average value of the all pixels is exported to the *3D pdf* file which is available electronically with this thesis in appendix 3.

6. Concluding remarks

6.1 Analysis and conclusions

A few important conclusions were drawn during this thesis which are presented below.

The camera calibration must be performed before every photogrammetric survey, because the intrinsic parameters of a submerged camera change significantly in comparison to the primary values. The focal length is larger and the Field of View is decreased underwater, thus a smaller area will be covered by a photograph then in the air. These changes should be taken into consideration during a preparation of a data acquisition plan. The data acquisition plan can be made based on assumed values calculated using approximate refraction index due to air-glass-water interface or using real values computed from the camera calibration procedure. The second procedure is recommended when a project is conducted based on the aerial photogrammetry principles and the underwater object is covered by vertical photographs. Due to the fact that the focal length and the Field of View parameters are very susceptible to the alterations in an underwater environment, the area that is covered by a single photograph can change and the overlap between photographs can turn out insufficient to achieve good stereo coverage. In that case the data acquisition plan should be created based on larger overlap or real values computed from the camera calibration procedure. If the close-range photogrammetry principles are used to measure the underwater object, that data acquisition plan can be created based on the approximate intrinsic camera parameters computed using an assumed refraction index. Additionally the underwater object should be covered by photographs from all sides to avoid bad object reconstruction. Furthermore the camera calibration should be performed from a close distance to the surveyed object, thus the environment will remain the same and intrinsic camera parameters will not change.

The underwater images are very dark and low quality, thus a few processing operations had to be performed: colour enhancement, haze removal and brightening of the image. These operations will improve an automatic photogrammetric point extraction conducted in Agisoft PhotoScan. The photographs were enhanced using both a script based on the Integrated Colour Model written by K. Iqbal and various functions from Photoshop Lightroom. The image processing performed in Photoshop Lightroom gave us better results than the first proposed technique. In contrast to the script, Photoshop allows us to use greater amount of adjusting parameters and in consequence get a result closest to the real appearance of the underwater object. The images processed in the script are too bright and too contrasted so they cannot be used in this project.

The underwater site should be illuminated evenly and no changes in brightness should occur between photographs. Significant differences will influence the automatic

photogrammetric point extraction process. If it is possible, no artificial light should be used. The lights often cause shadows on a scene which cover a part of the surveyed area and in result no data will be extracted there. In case when the artificial light had to be used more than one light should be used. The lights should be fixed symmetrically on the vehicle so that they should illuminate a larger area than image coverage. So the image will not only be bright in the centre of the image.

Due to the fact that any ground control points with known coordinates cannot be set up underwater, all other available methods that will provide us external data should be used. On the site a scale bar and vertical buoys should be used to scale the object and determine the horizontal direction. Underwater positioning systems and the extrinsic parameters of the stereo system unit will provide us the approximate position of the cameras during each exposure. This data can decrease a possibility of the object deformation which occurred in the pipeline model. Furthermore the surveyed area should be solid (square or rectangular) without any holes between the strips in order to avoid a problem which also occurred in pipeline measurement where one strip is protruding up with respect to the second one. On the other hand a measurement of the shovel which is based on the close range photogrammetry principles does not require additional external data. Only a use of the scale bar or vertical buoy is sufficient. The possibility of object deformation is highly decreased if the object is covered by photographs from the all sides.

The software which was responsible for taking simultaneous pictures failed. The left and the right camera were not taken photographs simultaneously. The difference between the exposures were not constant (around 0.1 second) and it was sufficient to influence the relative orientation of the stereo system unit. In consequence the extrinsic parameters of the stereo system could not be used. This software failure and a lack of data from the underwater positioning system resulted in no external data of both the objects.

Seaweed must be removed if we want to achieve a good and reliable three-dimensional model. The moving objects will influence the final result, especially if they cover the area of interest. Seaweed can also be removed from the dense cloud, however it will not produce a precise result. Seaweed which was hanging on the handle of the shovel was removed manually in the dense cloud, however created model was still not very accurate.

The construction of the three-dimensional model should be performed in a few software. Agisoft PhotoScan should be used to perform point extraction from the images and Geomagic should be used to clean the dense cloud and to create a three-dimensional model of the object. PhotoScan is highly advanced software which generates very accurate dense cloud, however the other features such as cleaning the dense cloud or building a mesh are very limited. Geomagic is more advanced 3D modelling tool in comparison to PhotoScan. This software allows us to choose from a variety of parameters and options to create the

three-dimensional model. Additionally Geomagic offers automatic repair of the model and very advanced hole closing tools. The texturizing of a model in Geomagic is performed manually and it is very time consuming. Especially in big projects this may significantly increase the processing time. Furthermore this algorithm does not work well if colours on the images differ from each other. When the object is photographed from different distances and angles, the illumination and colours on the images will change between the pictures. On the other hand texturizing in AgiSoft PhotoScan is completely automatic and very accurate. This software uses the positions of the cameras to set the image to the right position. In addition the colour correction algorithm works very well even on differently toned pictures. The whole 3D modelling process can be completely performed in Agisoft PhotoScan if a highly detailed result is not required. However if a highly detailed and accurate three-dimensional model is needed, the processes should be performed both in PhotoScan and Geomagic.

The remotely operated vehicle is very susceptible to any individual software and equipment failures. Despite the fact that the photogrammetry planning was very well prepared, due to technical problems the primary assumptions of this thesis was not fulfilled. Even so this project allowed us to understand more of the issues connected with underwater surveys and draw conclusions that should be implemented in further measurements.

6.2 Future work recommendation

Removal of seaweed covering the measured object is suggested in order to increase a quality of a model.

The underwater positioning system and the Inertial Measurement Unit (IMU) should be used to compute the approximate XYZ position and φ, ω, κ orientation data of the each camera position during exposure.

A pan/tilt unit freely movable in all directions should be used. Such a pan/tilt unit should allow us to arbitrary move a stereo bar in order to take both vertical and oblique photographs without a need to change the position of the entire rig during measurement.

Also improvements to the software used for camera synchronization is needed.

References

AIVL, Woods Hole Oceanographic Institut, 2012. TITANIC, What really happened, exclusive new photos of the week. *National Geographic*, April.

Allied Vision Technologies, 2013. *GC1380 - GigE Vision camera - High performance CCD camera with ExView HAD sensor.* [Online]
Available at: www.alliedvisiontec.com

APOMAB, A. o. P. M. a. B., 1999. *Underwater Acoustic Positioning System.* [Online]
Available at: http://www.hydro-international.com/download/whitepaper_uploadfile_9.pdf

AUVAC, A. U. V. A. C., 2014. *LBL Acoustic Positioning System.* [Online]
Available at: http://auvac.org/navigations/view/2
[Accessed 02 06 2014].

Behance, 2014. *ixtract | Titanic on Behance.* [Online]
Available at: http://www.behance.net/gallery/ixtract-Titanic/3422941
[Accessed 10 05 2014].

Bonin, F., Burguera, A. & Oliver, G., 2011. Imaging Systems for Advanced Underwater Vehicles. *Journal od Maritime Research,* VIII(1), pp. 65-86.

Bouguet, J.-Y., 2013. *Camera Calibration Toolbox for Matlab.* [Online]
Available at: http://www.vision.caltech.edu/bouguetj/calib_doc/htmls/parameters.html

Brager, S. & Chong, A. K., 1999. An application of close range photogrammetry in dolphin studies. *Photogrammetric Record,* Volume 16, pp. 503-517.

Chambah, M. et al., 2004. Underwater Color Constancy : Enhancement of Automatic Live Fish Recognition. *16th Annual symposium on electronic imaging.*

Diamanti, E., Georgopoulos, A. & Vlachaki, F., 2012. Geometric documentation of underwater archaeological sites. *XIII CIPA International Symposium.*

Drap , P., Durand, A., Provin, R. & Long, L., 2005. Integration of multi-source spatial information and XML information system in underwater archaeology. *CIPA XX International Symposium.*

Drap, P., 2012. *Underwater Photogrammetry for Archaeology, Special Applications of Photogrammetry.* s.l.:InTech.

Drap, P. et al., 2011. ROV-3D, 3D underwater survey combining optical and acoustic sensor. *The 12th International Symposium on Virtual Reality, Archaeology and Cultural Heritage VAST.*

Drap, P. et al., 2013. Automating The Measurement Of Red Coral In Situ Using Underwater Photogrammetry And Coded Targets. *International Archives of the Photogrammetry, Remote Sensing and Spatial Information Sciences,* Volume XL-5/W2, pp. 231-236.

Drap, P. et al., 2007. Photogrammetry for virtual exploration of underwater archeological sites. *Proceedings of the 21st International Symposium, CIPA 2007: AntiCIPAting the Future of the Cultural Past: Athens (Greece).*

Dunkan, F., Ludvigsen, M. & Sørensen, A. J., 2011. Dynamic Positioning System for a Small Size ROV with Experimental Results. *OCEANS, IEEE-Spain,* pp. 1-10.

Eric, M., Kovacic, R. & Berginc, G., 2013. The Impact of the Latest 3D Technologies on Documentation of Underwater Heritage Sites. *Digital Heritage International Congress, IEEE, Marseille,* p. 281–288.

Fryer, J. G., 1986. Lens distortion for close range photogrammetry. *ISPRS XXVI Real-time photogrammetry - a new challenge,* pp. 30-37.

Geomagic Studio 2014, 2014. *Goemagic Studio 2014 Online Help.* s.l.:Geomagic.

Harveya, E. et al., 2003. The accuracy and precision of underwater measurements of length and maximum body depth of southern bluefin tuna (Thunnus maccoyii) with a stereo–video camera system. *Fisheries Research 63,* pp. 315-326.

Havrey, E. et al., 2003. The accuracy and precision of underwater measurements of length and maximum body depth of southern bluefin tuna (Thunnus maccoyii) with a stereo–video camera system. *Fisheries Research 63,* pp. 315-326.

Heikkilä, J. & Silven, O., 1997. A Four-step Camera Calibration Procedure with Implicit Image Correction. *IEEE,* pp. 1106-1112.

Henderson, J., Pizarro, O., Johnson-Roberson, M. & Mahon, I., 2013. Mapping submerged archaeological sited using stereo-vision photogrammetry. *The International Journal of Natutical Archaeology,* Volume 42, pp. 243-256.

Iqbal, K., Salam, R. A., Osman, A. & Talib, A. Z., 2007. Underwater image enchancement using an integrated colour model. *IAENG International Journal of Computer Science.*

Jasinski, M. E., Sortland, B. & Søreide, F., 1995. Applications of remotely controlled equipment in norweian marine archeology. *Oceans'95,* pp. 566-572.

Johannessen, R. & Prytz, F., 2005. *Hydro International, surveying in all waters.* [Online] Available at: http://www.hydro-international.com/issues/articles/id564-

Underwater_Metrology.html
[Accessed 10 2005].

Jordt-Sedlazeck, A. & Koch, R., 2012. Refractive Calibration of Underwater Cameras. In: *Lecture notes in computer science.* s.l.:s.n., pp. 846-859.

Karpel, Y. Y. & Schlechner, N., 2005. Recovery of Underwater Visibility and Structure by Polarization Analysis. *IEEE Journal of Oceanic Engineering,* 30(3), pp. 570-587.

Knight, D., 2011. *Artificial Lighting for Underwater Photography.* [Online]
Available at: http://www.camerasunderwater.co.uk/articles/lighting/lighting-techniques

Kreuznach, S., 2014. *3 Mega Pixel lens Cingon 1.4/8.* [Online]
Available at:
http://www.schneiderkreuznach.com/fileadmin/user_upload/bu_industrial_solutions/industrie
optik/11mm_Lenses/3MP_Compact_Lenses/Cinegon_1.4-8.pdf
[Accessed 23 04 2014].

Kwon, Y.-H., 1998. *Refraction error.* [Online]
Available at: http://www.kwon3d.com/theory/dlt/refr.html

Lavest, J. M., Rives, G. & Lapreste, J. T., 2003. Dry camera calibration for underwater applications. *Machine Vision and Applications,* pp. 245-253.

Lens, A., 2011. *Agisoft Lens User Manual version 0.4.0.* s.l.:s.n.

Ludvigsen, M., 2010. *An ROV toolbox for optical and acoustical seabed investigations, Thesis for the degree of philosophiae doctor.* Doctoral Theses at NTNU, 2010:74 ed. Trondheim: s.n.

Ludvigsen, M. et al., 2013. Scientific operations combining ROV and AUV in the Trondheim Fjord. *OCEANS-Bergen, 2013 MTS/IEEE,* pp. 1-7.

Luhmann, T., Robson, S., Kyle, S. & Harley, I., 2006. *Close range photogrammetry.* s.l.:Whittles Publishing.
MathWorks, 2012. *Matlab help - Image Processing Toolbox.* s.l., s.n.

MCE Ch. II §3, 1978. *Act of 9 June 1978 No.50 Concerning the Cultural Heritage Ch. II §3, Prohibition against disturbing monuments and sites.* s.l.:s.n.

MCE Ch. IV §10, 1978. *Act of 9 June 1978 No.50 Concerning the Cultural Heritage Ch. IV §10, Prohibition against disturbing monuments and sites.* s.l.:s.n.

Nowakowski, A. & Skarbek, W., 2013. *Analysis of Brown camera distortion model.* s.l., s.n.
NTNU, N. U. o. S. a. T., 2014. *R/V Gunnerus.* [Online]
Available at: http://www.ntnu.edu/marine/gunnerus

NTNU, N. U. o. S. a. T., 2014. *ROV Minerva.* [Online]
Available at: http://www.ntnu.edu/marine/minerva

Ødegård, Ø., Ludvigsen, M. & Lågstad, P. A., 2013. Using synthetic aperture sonar in marine archaeological surveys-Some first experiences. *OCEANS-Bergen, 2013 MTS/IEEE,* pp. 1-7.
PhotoModeler Help Topics, 2013. s.l.:s.n.

Photoscan, A., 2013. *AgiSoft PhotoScan Help.* s.l.:s.n.

Remondino, F. F. C., 2006. Digital camera calibration methods: considerations and comparisions. *ISPRS Commission V Symposium 'Image Engineering and Vision Metrology.*

Sedlazeck, A. & Koch, R., 2011. *Calibration of Housing Parameters for Underwater Stereo-Camera Rigs.* s.l., s.n.

Shortis, M., Havrey, E. & Seager, J., 2007. *A Review of the status and trends in underwater videometric measurement.* San Jose, California, SPIE Conference 6491, Videometrics IX,.

Shortis, M. R. & Harvey, E. S., 1998. Design and calibration of an underwater stereo-video system for the monitoring of marine fauna populations. *International Archives*, pp. 792-799.
Skarlatos, D., Agapiou, A. & Rova, M., 2010. Photogrammetric support on an underwater archeologica excavation site: The Mazotos shipwreck case. *Euromed digital heritage conference.*

Skarlatos, D. & Rova, M., 2010. Photogrammetric approaches for the archaeological mapping The Mazotos shipwreck. *Euromed 2010, Digital Heritage.*

Søreide, F., 2000. Cost-effective deep water archaeology: preliminary investigations in Trondheim Harbour. *The International Journal of Nautical Archaeology,* pp. 284-293.

Søreide, F., 2011. *Ships from the Depths: Deepwater Archaeology.* College Station, TX, USA: Texas A&M University Press.

Systems, S., 2014. *What are your means of positioning the ROV?.* [Online]
Available at: http://www.seaviewsystems.com/questions/what-are-your-means-of-positioning-the-rov/
[Accessed 02 06 2014].

Telem, G. & Filin, S., 2010. Photogrammetric modeling of underwater environments. *ISPRS Journal of Photogrammetry and Remote Sensing,* Volume 65, pp. 433-444.

Thompson, M. . M., 1966. American Society of Photogrammetry and Remote Sensing's: Manual of Photogrammetry 3rd edition. In: s.l.:s.n.

UNESCO, 2011. *The Convention on the Protection of Underwater Cultural Heritage.* s.l.:s.n.

Zuchovsky, M. O., Kuznetsov, V. D. & Olkhovsky, S. V., 2013. Photogrammetric techniques for 3-D underwater record of the antique time ship from phanagoria. *International Archives of the Photogrammery, Remote Sensing and Spatial Information Sciences,* Volume XL-5/W2.